The Solar Mass Ejection Imager Optics and Baffles – Design and Construction

Bernard V. Jackson
Andrew Buffington
P. Paul Hick

University of California at San Diego
9500 Gilman Drive
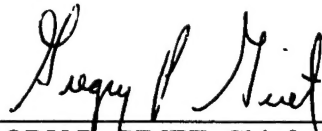La Jolla, CA 92093-0424

15 Nov 2000

Final Report

AIR FORCE RESEARCH LABORATORY
Space Vehicles Directorate
29 Randolph Rd
AIR FORCE MATERIEL COMMAND

20020124 418

" This technical report has been reviewed and is approved for publication."

_____
JANET C. JOHNSTON
Contract Monitor

_____
GREGORY P. GINET, Chief
Space Weather Center of Excellence

REPORT DOCUMENTATION PAGE			Form Approved OMB No. 0704-0188

Public reporting burden for this collection of information is estimated to average 1 hour per response, including the time for reviewing instructions, searching existing data sources, gathering and maintaining the data needed, and completing and reviewing the collection of information. Send comments regarding this burden estimate or any other aspect of this collection of information, including suggestions for reducing this burden, to Washington Headquarters Services, Directorate for Information Operations and Reports, 1215 Jefferson Davis Highway, Suite 1204, Arlington, VA 22202-4302, and to the Office of Management and Budget, Paperwork Reduction Project (0704-0188), Washington, DC 20503.

1. AGENCY USE ONLY (Leave Blank)	2. REPORT DATE 15 November 2000	3. REPORT TYPE AND DATES COVERED Final Report	

TITLE AND SUBTITLE
The Solar Mass Ejection Imager Optics and Baffles - Design and Construction

5. FUNDING NUMBERS
Contract: F19628-96-C-0054
PE 69120J
PR 7601
TA 70
WU AD

6. AUTHORS
Bernard V. Jackson, Andrew Buffington, P. Paul Hick

7. PERFORMING ORGANIZATION NAME(S) AND ADDRESS(ES)
The Regents of the University of California
University of California, San Diego

8. PERFORMING ORGANIZATION REPORT NUMBER

9. SPONSORING / MONITORING AGENCY NAME(S) AND ADDRESS(ES)
The Air Force Research Laboratory (AFRL/VSBS)
29 Randolph Road
Hanscom AFB MA 01731-3010

Contract Manager: Janet Johnston/VSBX

10. SPONSORING / MONITORING AGENCY REPORT NUMBER
AFRL-VS-TR-2001-1515

11. SUPPLEMENTARY NOTES

12a. DISTRIBUTION / AVAILABILITY STATEMENT
Approved for public release;
Distribution unlimited

12b. DISTRIBUTION CODE

13. ABSTRACT (Maximum 200 words)
The purpose of SMEI is a proof-of-concept of the ability to predict geomagnetic disturbances for Air Force space operations and to establish the feasibility of tracking interplanetary disturbances from the Sun to the Earth and beyond. The major subsystems of SMEI are an electronic Camera Assembly, a Data Handling Unit and interconnection harnesses. Each electronic Camera component consists of a baffle, radiator, bright object sensor, strongbox (CCD, mirrors and shutter) and electronics box. The electronic Camera Assembly is used to observe in visible light mass ejections from the Sun by sensing sunlight scattered from clouds of solar-produced interplanetary electrons. Predictions of arrival time at Earth of this disturbance can be made up to three days in advance.

14. SUBJECT TERMS
Coronal mass ejection, Geomagnetic Storms, Space Weather

15. NUMBER OF PAGES
5 (4 Appendicies)

16. PRICE CODE

17. SECURITY CLASSIFICATION OF REPORT UNCLASSIFIED	18. SECURITY CLASSIFICATION OF THIS PAGE UNCLASSIFIED	19. SECURITY CLASSIFICATION OF ABSTRACT UNCLASSIFIED	20. LIMITATION OF ABSTRACT SAR

NSN 7540-01-280-5500

Standard Form 298 (Rev. 2-89)
Prescribed by ANSI Std. Z39-1
298-102

The Solar Mass Ejection Imager Optics and Baffles - Design and Construction

1.   Introduction

The SMEI objective is to develop and fly an all-sky Camera Assembly capable of measuring solar mass ejections as they propagate through the interplanetary medium. To this end we must develop methods to use these data to give 1-3 day advance warning of geomagnetic disturbances that disrupt and destroy DoD operations and assets in space. The experiment views almost 4 π steradians of sky and will map space around Earth and towards the Sun providing arrival time predictions of mass ejections from the Sun up to three days in advance. Furthermore, the experiment will track the solar ejecta and collect data as the mass leaves the near-Earth environment (passes the Earth) and moves into deep space.

SMEI will operate continuously in an automatic mode. Data from the electronic Camera Assembly will be digitized within the experiment and delivered to the space vehicle for recording and downlinking at a constant rate of approximately 55 kilobits per second. Shortly after launch (and after out-gassing of the spacecraft has dropped to an acceptable level) the SMEI experiment will be activated via ground command.

2.   Progress

During this contract, the SMEI baffles designed by UCSD and subcontracted to be blackened by Martin-Lockheed near Denver were delivered to Birmingham, England. The UCSD prototype of this system was tested and was shown to acceptably decrease sunlight by over 9 orders of magnitude with the Sun within 18° of baffle narrow field of view and to within 28° in the baffle wide dimension as designed. The SMEI flight optics including the SMEI mirrors subcontracted to Hyperfine of Boulder, Colorado were designed and delivered. We certified the prototype M1 (primary mirror) and M2 (secondary mirror) design using the SMEI prototype CCD camera. Laboratory tests certified that the optics and our CCD camera are capable of the 0.1% photometry specification. We built a UCSD tomography program to operate both in corotating and in a 'time-dependent' mode using the Helios photometer and interplanetary scintillation (IPS) data so that rotating solar structures and outward plasma motion alone can provide the perspective views required to deconvolve plasma structure densities. These structures include CMEs as well as other corotating and transient features.

2.1.   SMEI Prototype Baffle Tests

The SMEI baffle that was designed at UCSD was shown to work correctly during this contract period. Extensive testing of the SMEI prototype baffle (Appendix II and Appendix IV) show the baffle to operate to nearly the design specification. A slight degradation of the prototype baffle performance caused by a poorer than specified contracted blackened surface has reportedly been

corrected in the subsequent flight baffle blackened surfaces. There was also a previously uncalculated double diffraction path discovered in prototype baffle testing. This light path to the SMEI imaging optical surfaces is another of the limiting stray light processes in the SMEI baffles.

2.2. SMEI Optics Alignment

The SMEI flight optics (baffles, mirrors and CCD) require alignment certification relative to themselves and to the spacecraft prior to flight. This had not been done as of the final report date for this contract.

2.3. SMEI CCD Prototype Camera Tests

During this contract the SMEI prototype CCD camera was designed, delivered to UCSD and operated to characterize the SMEI optics design and to certify that the optical system and CCD are capable of achieving a 0.1% photometric specification if used in conjunction with the SMEI mirrors. A portion of the tests used to determine the CCD camera specifications are given in Appendix I.

2.4. SMEI Flight Optics Mirrors

Near the end of the contract period the final acceptable SMEI diamond-turned mirror flight optical design from Hyperfine of Boulder, Colorado was delivered to UCSD. The problems on earlier versions of the subcontracted design that had been delivered to UCSD were overcome or reduced considerably on the final mirrors sent. The accepted mirror optical design and each of the flight mirrors have been certified to achieve the 0.1% photometric specification in laboratory tests (in December 2000) for small motions of bright point sources relative to the instrument optical axis. Scattering in the primary M1 mirror narrow dimension is greater than anticipated, and this primarily affects bright stellar signals as they transit beyond the instrument field of view. At the time of this report, it is not clear to what degree this will affect ultimate SMEI performance. The clean room control requirements that mainly affect SMEI optics and the contamination of them prior to a during spaceflight are given in Appendix III.

2.5. SMEI Vane V

The new vane V design (in September 2000) was manufactured at UCSD, tested for optical properties and delivered to our laboratory at the end of the contract. This new vane (which acts as a Lyot stop) is a significant improvement over the earlier SMEI optics designs.

2.6. Software

There was work on two types of software during the period of this contract. A software program that allowed an accurate image registration, calibration and background to be subtracted from around each laboratory image point source was used to certify the SMEI prototype CCD and

optics. This preliminary version of the SMEI image analysis software gives considerable insight into how accurate (and difficult) it will be to provide precise photometric (0.1%) SMEI images in real time from space.

Work on tomographic software that will allow an accurate forecast of heliospheric structure arrival at Earth was designed and operated during this contract period. The tomographic program now operates in a "time-dependent" version that assumes that the heliosphere evolves over time and that structures in it can evolve temporally over periods as short as one day. This program has been used to analyze archival Cambridge, England IPS data currently-available STELab IPS data available from Nagoya University, Japan and Helios photometer data available at UCSD. More work on the time-dependent version of the Helios photometer analysis has demonstrated in its use for mapping the 3-D structure of CMEs and in accurately calibrating these structures such as CMEs when they are mapped to in-situ observations near the observer.

2.7. Publication Status

A partial listing of the publications that acknowledge or are related to this Air Force contract follow:

Abstracts/References

1. Jackson, B.V. and P. Hick, "Three Dimensional Tomography of Heliospheric Features Using Global Thomson Scattering Data", COSPAR XXXII meeting, Nagoya, Japan, 14-19 July (1998).

2. Jackson, B.V., A. Buffington, P. Hick, S.L. Keil, R.C. Altrock, S. Kahler, G. M. Simnett, C.J. Eyles and D. Webb, "The solar mass ejection imager (SMEI)", to the Proceedings of the SPIE 3442 (1998). +

3. Jackson, B.V., P.P. Hick, R.A. Howard and K.P. Dere, "Background coronal speeds from correlation techniques applied to LASCO images", presented at Solar Wind 9 held on Nantucket Island, Massachusetts, 5-9 October (1998).

4. Buffington, A., Hick, P.P. and Jackson, B.V., "Visible-light All-sky Imagers in Deep Space", BAAS 31 (3), 959, 1999.

5. Jackson, B.V., Hick, P.P. and Buffington, A., "Recent UCSD Advances in Tomography for Use with Heliospheric Remote-Sensing Data", BAAS 31 (3), 958, 1999a.

6. Jackson, B.V., Hick, P.P. and Buffington, A., "Recent UCSD advances in 'time dependent' tomography for use with heliospheric remote-sensing data", presented at the SHINE 99 Workshop, June 14-18, 1999b.

7. Hick, P.P., B.V. Jackson, and A. Buffington, "Heliospheric Tomography: Reconstruction from Remote Sensing Observations", EOS, 80, F790 (1999).

8. Dunn, T, B.V. Jackson, P.P. Hick and A. Buffington, "Forecasting Solar Wind Parameters Using IPS Tomography, *EOS*, 80, F790 (1999).

9. Jackson, B.V., Hick, P.P. and Buffington, A., "Mapping Heliospheric CMEs Using Tomographic Techniques", *EOS*, **80**, F810, (1999).

10. Killen, R.M., B.L. Giles, P.H. Reiff, B.V. Jackson and A. Lukyanov, "Space Weather at Mercury", *EOS*, **80**, F897 (1999).

Reports, Conference Proceedings

1. Goldstein, B.E., A. Buffington, A.C. Cummings, R. Fisher, B.V. Jackson, P.C. Liewer, R.A. Mewaldt and M. Neugebauer, "Solar polar sail mission: report of a study to place a spacecraft in a polar orbit around the sun", *Proc. SPIE 3442*, 65 (1998) (12 pages).

2. Buffington, A., P. Hick, B.V. Jackson and C.M. Korendyke, "Corrals, hubcaps, and crystal balls: some new designs for very wide-angle visible-light heliospheric imagers", *Proc. SPIE 3442,* 77 (1998) (10 pages).

3. Hick, P. and B.V. Jackson, "Three-dimensional tomography of heliospheric features using Thomson-scattering data", *Proc. SPIE 3442*, 87 (1998) (7 pages).

4. Buffington, A., "Stray-light rejection results with the SMEI prototype baffle", *SMEI MEMO* (October 16, 1998) (11 pages). +

5. Buffington, A., "0.1% Heliospheric Imager Integration Times", (February 12, 1999) (3 pages) *UCSD MEMO*.

6. Buffington, A., "An improved Design for Stray-Light Reduction with a Hemispherical or Larger Imager", (December 10, 1999) (5 pages) *UCSD MEMO*.

Research Articles

1. Jackson, B.V., P.L. Hick, M. Kojima and A. Yokobe, "Heliospheric Tomography Using Interplanetary Scintillation Observations 1. Combined Nagoya and Cambridge data", *J. Geophys. Res.*, **103**, 12,049 (1998) (19 pages).

2. Kojima, M., M. Tokumaru, H. Watanabe, A. Yokobe, K. Asai, Jackson, B.V., and P.L. Hick, "Heliospheric Tomography Using Interplanetary Scintillation Observations 2. Latitude and Heliocentric Distance Dependence of Solar Wind Structure at 0.1-1 AU", *J. Geophys. Res.*, **103**, 1981 (1998) (9 pages).

3. Asai, K., M. Kojima, M. Tokumaru, A. Yokobe, B.V. Jackson, P.L. Hick, and P.K. Manoharan, "Heliospheric Tomography Using Interplanetary Scintillation Observations 3.

The Velocity Dependence of Electron Density Fluctuations in the Solar Wind", *J. Geophys. Res.*, **103**, 1991 (1998) (9 pages).

4. Buffington, A., "Very-wide-angle optical systems suitable for spaceborne photometric measurements", *Applied Optics*, **37**, No. 19, 4284 (1998) (10 pages). +

5. Leinert, Ch. and B.V. Jackson, "Global Heliospheric Solar Wind Changes Over Solar Cycle 21: a Comparison of Helios Photometer, In-situ and IPS data", *Astrophys. J.*, **505**, 984 (1998) (9 pages).

6. Hick, P., Z.Svestka, B.V. Jackson, F. Farnik and H.S. Hudson, "Quiet Solar Wind Signatures Above Active Regions Observed in X-rays", in *Solar Wind Nine*, S.R. Habbal, R. Esser, J.V. Hollweg and P.A. Isenberg, eds., AIP Conference Proceedings 471, Woodbury, 231, (1999) (3 pages).

7. Yokobe, A., T. Ohmi, K. Hakamada, M. Kojima, M. Tokumaru, B.V. Jackson, P.P. Hick and S. Zidowitz, "Comparison of Solar Wind Speed with Coronagraph Data Analyzed by a Tomography", in *Solar Wind Nine*, S.R. Habbal, R. Esser, J.V. Hollweg and P.A. Isenberg, eds., AIP Conference Proceedings 471, Woodbury, 565, (1999) (3 pages).

8. Buffington, A., "Improved Design for Stray-Light Reduction with a Hemispherical Imager", *Applied Optics*, **39**, 2683 (2000) (4 pages).

7. Jackson, B.V. and P. Hick, "Three Dimensional Tomography of Heliospheric Features Using Global Thomson Scattering Data", *Adv. in Space Res.*, **25**, No. 9, 1875, 2000 (4 pages).

+ Acknowledges Current Contract F19628-8-96-C0054

Appendix I

Measurements of Subpixel Gradients for the EEV CCD 05-02

MEASUREMENTS OF SUBPIXEL GRADIENTS
FOR THE EEV CCD 05-20

Andrew Buffington
Center for Astrophysics and Space Sciences
University of California, San Diego
La Jolla. CA 92093-0424
(619)-534-6630

19 February 1997

I.   INTRODUCTION

Choosing a CCD chip for the Solar Mass Ejection Imager (SMEI) is an important milestone. Our memos dated 17 February 1993 and 24 January 1994 present subpixel gradient measurements of the Thomson TH7863 CCD chip, and show this would likely deliver 0.1% photometry required for SMEI. However, its format is too small for the field of view, even with a redesign to reduce area (memo 7 May 1996).

The redesign was for a 28.7 mm long Thomson TH7899, but with minor adjustment is probably suitable for a 28 mm long EEV05-30. Electronics design is available for this, adaptable for SMEI. This memo presents results of a subpixel gradient measurement using a closely related EEV05-20 chip. We find a subpixel-gradient contribution to the photometric error budget comparable to the TH7863, thus implying this chip is also suitable for SMEI.

II.   MEASUREMENT SETUP

The earlier measurement technique used Offner optics to relay a field of bright squares onto the TH7863 CCD at 1:1 magnification. The image was moved over the pixels by hanging weights on the optical bench; motion was determined from the squares centroid positions. This setup provides good image quality compared with the TH7863's 23μ pixel size. However, the setup is difficult to transport to other locations, and probably provides an "overkill" in image quality compared with SMEI images.

With 22.5μ pixels, the EEV05 family is closely similar to the Thomson TH7863. Nick Waltham, head of the CCD group at Rutherford Appleton Laboratory in Chilton Didcot, England, kindly invited us to use one of his CCD cameras to measure subpixel properties for SMEI. Peter Anderson and I did so on 22-23 January 1997.

To avoid transporting Offner optics we prepared a white-paper lined box containing a halogen bulb, several diffusing screens, and a 1.6 mm thick aluminum plate on the front having a grid of 9 x 15 1 mm diameter holes spaced at 12.7 mm intervals. A second plate has 5 x 8 10.5 mm holes at 25.4 mm intervals. The diffusing screens enabled uniform illumination to about ±20%. The box is mounted on two micrometer slides for motion in the plane of the front plate.

8

The pattern of bright spots on a dark background is viewed by a standard camera lens, in this case the one already on Nick's camera. Demagnification of about 20:1 enables reproducible positioning within a small fraction of a pixel, directly readable from the micrometer knobs. The lines of spots are aligned parallel to pixel-edge lines and the slides translate the spots respectively perpendicular to the CCD read lines, and to the CCD channel stops.

The bulb is powered by a regulated power supply; each data frame is normalized in the analysis to remove typical 0.5% changes in bulb illumination, and remove ten times smaller variations in the background illumination between the spots.

The setup remeasured our Thomson TH7863 here at UCSD, then the EEV05-20 at Nick's lab in England. In both cases, the standard green filter used in the earlier 1993 work was installed, even though maybe unnecessary, since little of the "long infrared tail" of light from the halogen bulb should leak through the thick aluminum plate. Distance from plate to lens is adjusted to make the 12.7 mm between hole centers exactly 32 pixels on the CCD. The small holes are 2.52 pixels in diameter on the CCD, and thus easily separated for measurement of photometric response versus position.

The TH7863 shows a roughly sinusoidal variation for each spot as a function of position. The plate is moved in steps of 1/8 pixel. Perpendicular to the channel stops, peak-to-peak response variation is ~0.6%, as expected scaling from the earlier TH7863 measurement. Random r.m.s. residual is about 1/3 of this.

The large holes are 26.45 pixels in diameter, larger than the roughly 20-pixels-on-a-side SMEI images (figure 5 of the 7 May 1996 memo), and significantly less structured. We expect photometric variation, as these spots are moved, well below the 0.1% SMEI specification. Moving the TH7863 perpendicular to its channel stops, its direction of greatest photometric susceptibility, one-pixel periodic variation is less than ±0.02%, and many spots are close to the ±0.01% limit set by photoelectron counting statistics.

III. RESULTS FOR THE EEV05-20

A. Perpendicular to the channel stops

Figure 1 shows the fractional photometric deviation for the spot in the center of the small-spot grid, for motion perpendicular to channel stops. A fitted sinusoid with slope is also shown. Comparable sinusoid amplitudes are found for all spots, although these drop off somewhat away from the optical axis, presumably due to varying focus quality over the field of view. This EEV chip shows average periodic variation amplitudes of 0.4%, and random r.m.s. residuals of 0.3%. Photoelectron counting noise for this measurement is about 0.1%. These values are a factor of about 1.5 times larger than the equivalent numbers for the Thomson TH7863.

The large spots have periodic photometric amplitudes and r.m.s. residues of 0.015%, about the same as for the Thomson chip. Photoelectron noise here is 0.010%, so the true periodic amplitudes and residues are reduced to about 0.01%. SMEI's smaller and more structured images should be a factor of several worse than this.

B.   Perpendicular to the read lines

Figure 2 shows small-spot fractional photometric deviation perpendicular to the read lines. Here the periodic variation is twice larger than figure 1, but the random residue is the same.

The large spots have periodic photometric amplitudes of about 0.02%, and residues of 0.015%. Thus random photometric variation is about 0.01%, the same in both directions, while periodic variation is comparable to this perpendicular to the channel stops, and double this perpendicular to the read lines.

IV.   DISCUSSION

The above measurements do not directly measure subpixel gradients, but they do measure closely related r.m.s. response-variation averages. The 7 May 1996 memo relates these averages to expected SMEI performance for both periodic and random variations. In summary, r.m.s. subpixel variations less than about 5% are averaged by SMEI images down below 0.05%, the amount included for this contribution in the SMEI error budget. Perpendicular to the channel stops, the above EEV05 measurements imply a several percent r.m.s. variation within a pixel, thus acceptable for SMEI.

Perpendicular to the read lines, measured variation is about twice larger. However, the SMEI images smear during an exposure as the zenith vector sweeps through the sky. Median smearing is about 3 pixels. Configuring the EEV05 chip for SMEI, the smearing direction is always within ±30° of perpendicular to the read lines. The 7 May 1996 memo evaluates smearing: this reduces the periodic effect by about a factor of six, more than enough to compensate for the above twice larger amplitudes. **Thus the chip is acceptable for SMEI in both dimensions, and may even have a comfortable margin perpendicular to the read lines.**

V.   CONCLUSION

This EEV05 measurement shows this chip is nearly as good as the Thomson TH7863 for the 0.1% SMEI photometry. The large-spot data directly confirm this for both chips.

Whether an EEV05-30 chip will actually prove satisfactory for SMEI depends on the assumption that individual chips of the family perform comparably and no important further source of noise crops up. We note also that the CCD operating temperature is still open: CCD dark/read noise is likely an important error budget contributor.

Figure 1. EEV05-20 fractional photometric deviation plotted as a function of pattern position perpendicular to the channel stops, for a _single spot_ at the center of the test pattern. Sinusoidal variation is due to the spot moving over response variations resulting from the periodic CCD channel stop structures. All spots show qualitatively similar behavior.

Smooth curve: least-squares fit to a sloped sinusoid.

Individual data frames (each position along the X-axis above) have been corrected for variation in overall illumination and variation in background beneath each spot.
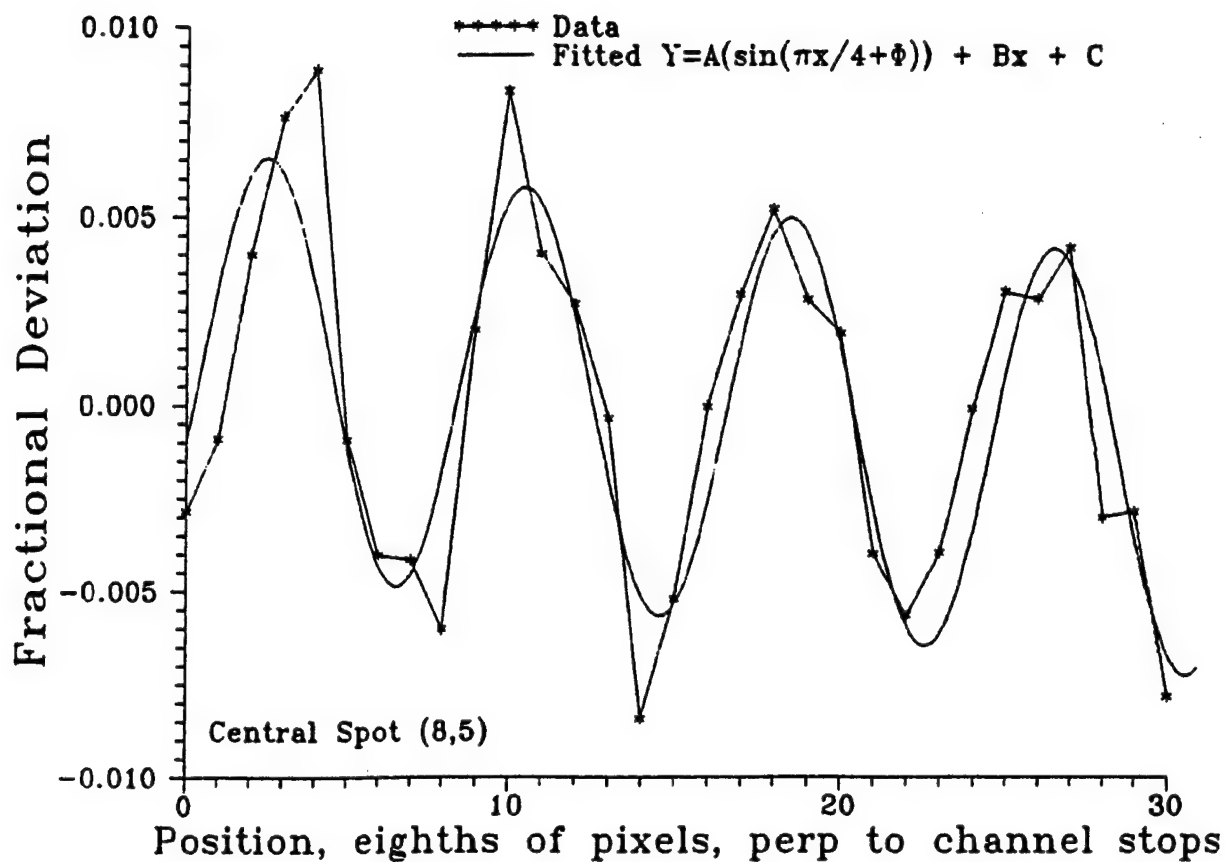
11
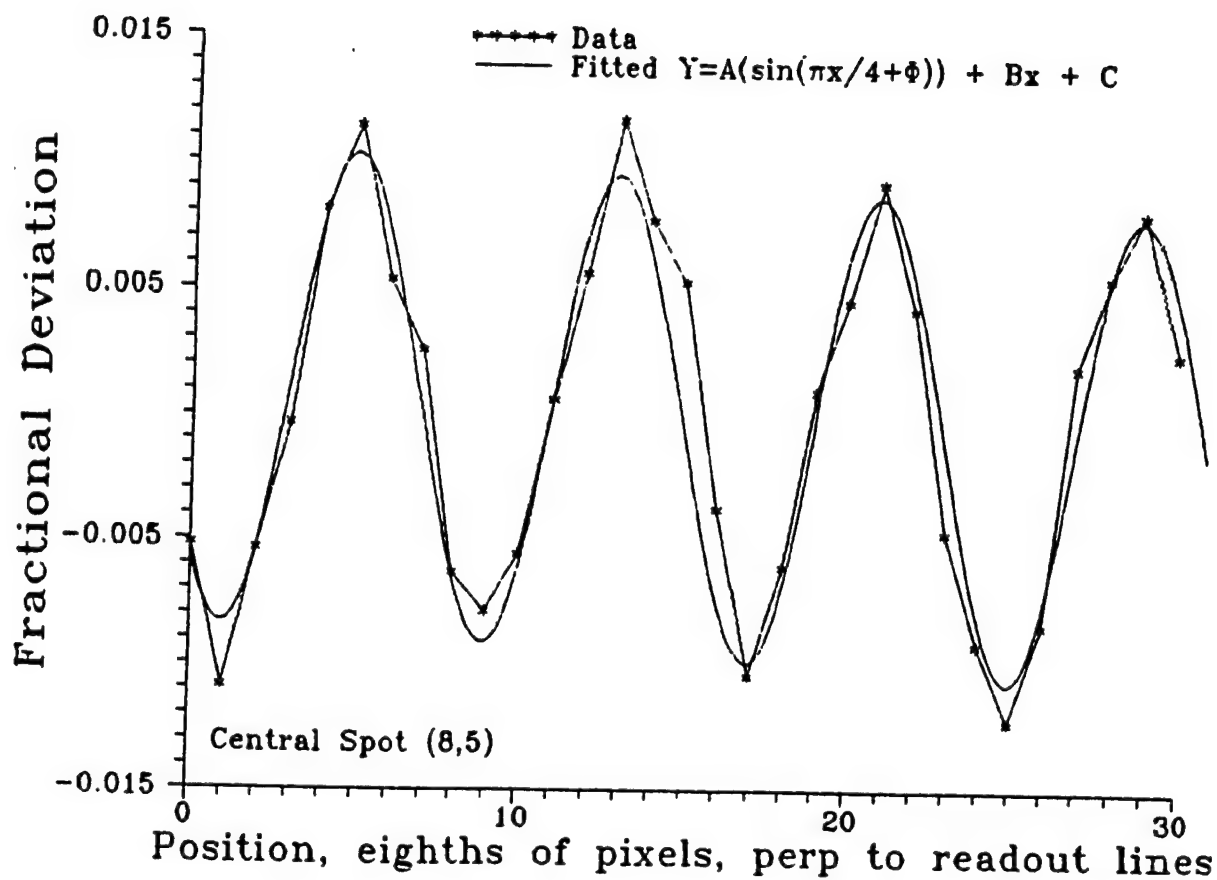
Figure 2. EEV05-20 fractional photometric variation plotted as a function of pattern position perpendicular to the read lines, for a single spot at the center of the test pattern. Sinusoidal variation is due to the spot moving over response variations resulting from the periodic CCD readout line and implant structure. Smooth curve: least-squares fit to a sloped sinusoid.

Appendix II

Measuring Stray-Light Rejection for the SMEI Prototype Baffle

MEASURING STRAY-LIGHT REJECTION FOR THE SMEI PROTOTYPE BAFFLE

Andrew Buffington
Center for Astrophysics and Space Sciences
University of California, San Diego
La Jolla, CA 92093-0424

April 28, 1998

I. INTRODUCTION

The Solar Mass Ejection Imager (SMEI) will measure heliospheric features which are typically 1% or less of the ambient zodiacal light and starlight. To enable quantitative measurements of such low-contrast features, the instrument optics must be well protected from stray sunlight scattering into the primary aperture. The SMEI baffle accomplishing this consists of a pyramidal structure surrounding the optical viewing column, with numerous vanes which both block the most direct scattering paths and absorb the light. The interior of the baffle has a Martin Black coating absorbing all but $\eta = 0.5\%$ of incident light (Pompea and McCall 1992). For near-perpendicular incidence the re-radiated light is close to Lambertian (Breault 1977). The design ensures that light entering the baffle beyond about 20° from the center line, in the direction of the field of view's narrow dimension, must rescatter at least three times before it reaches the optics entrance aperture. Baffle performance is thus proportional to between η^3 and η^4; the design promises better than 10^{-10} rejection of stray light relative to direct solar illumination of the SMEI aperture. A prototype baffle is built and presently receiving its black coating. This memo describes the setup for measuring its stray-light rejection, and discusses the capabilities and limits of our technique.

II. LABORATORY SETUP

Figure 1 shows the setup. A collimated light-source beam provided by a Fairchild 122 cm focal length f6.3 lens with a 1 cm illuminated aperture at its focal plane illuminates a portion of the front (vane 8) of the baffle. For each incident angle the beam width is masked to just larger than the opening in the baffle. Light enters the baffle opening, where in the 45° case illustrated here it illuminates portions of the outsides of the next two vanes, and of the outermost three septum bottoms. Some of this light is re-radiated and works its way deeper into the baffle. A photomultiplier placed behind aperture A measures the amount of light finally making it through A. The measurement is normalized by illuminating A directly, with light incident at 0° but greatly attenuated with neutral-density filters.
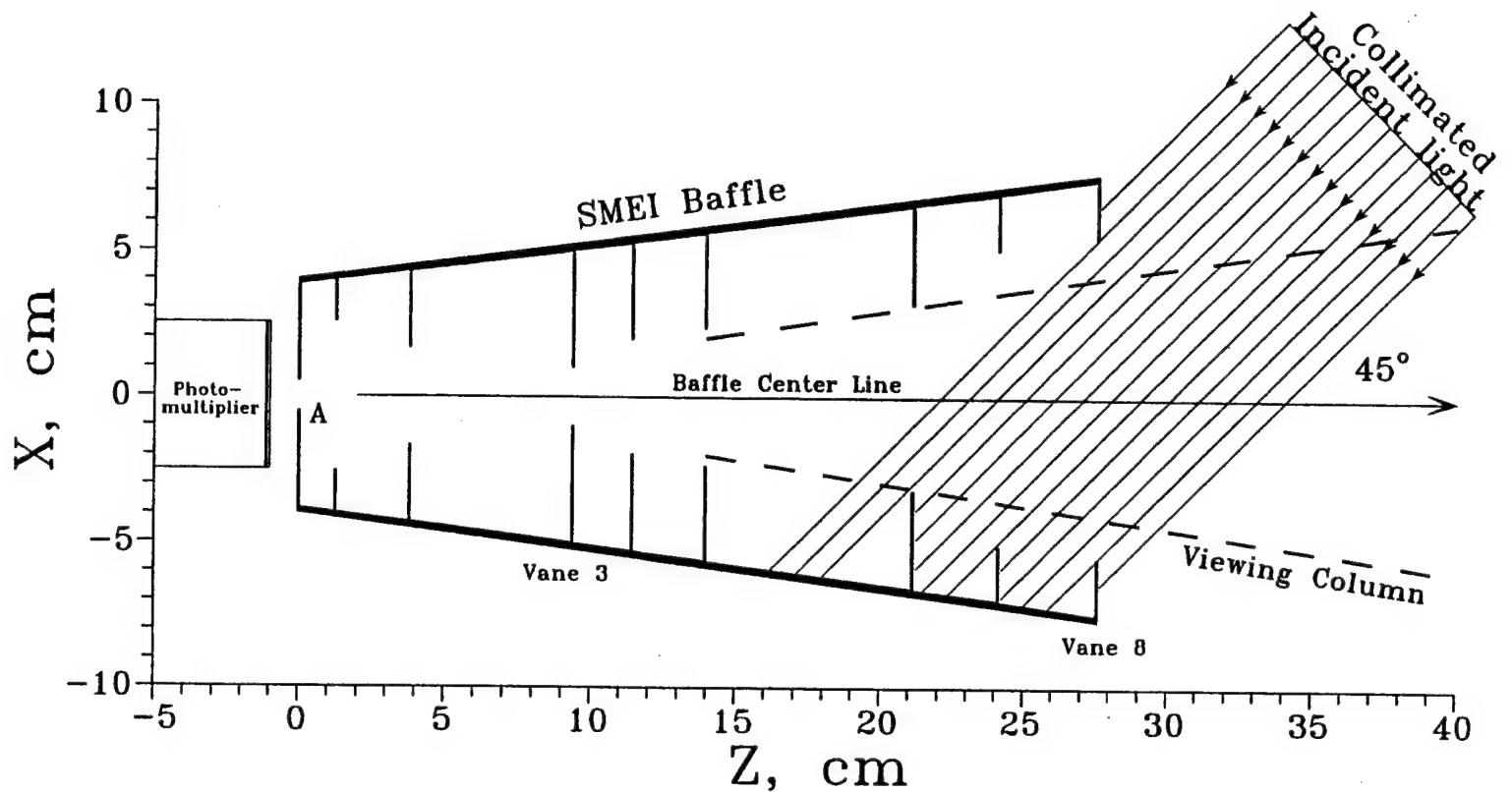
Figure 1. A schematic diagram of the SMEI baffle stray-light test setup. The setup is shown for measuring light rejection in the plane of the baffle's narrow dimension. Parallel light enters at angle θ, shown here at 45°, and illuminates a portion of the baffle interior. Some of it passes through aperture A after scattering several times, where it is measured by a photomultiplier. The interior of the baffle is coated with Martin Black. Dashed lines indicate the pyramidal "viewing column", the volume directly visible by the photomultiplier; this volume extends beyond the right-hand side of the figure, eventually terminating in a black panel. The baffle is designed to provide better than 10^{-10} rejection of sunlight having θ ≥ 20°.

The photomultiplier directly views everything beyond vane 3 contained within a volume defined by the peripheries of aperture A and of vane 3. This volume is roughly pyramidal with its apex close to A and with opening half-angles of about 8° and 35° respectively, in the baffle's short and long dimensions. This "viewing column" is terminated off to the right of figure 1, with a dark panel which is part of the test setup. Scattered light also enters the viewing column from the front of vane 8 or coming back out from within the baffle through the vane 8 opening. Any light reaching the terminating panel inside of the viewing column can scatter from there directly into aperture A and be detected. Therefore, a key element of this setup is the placement and blackness of the material chosen for the terminating panel. As a practical consideration, enclosing this volume also on its sides controls potential entry of stray laboratory light, important considering the low light levels being detected here.

Assume that the terminating panel is planar, perpendicular to the baffle center line, and at distance D from aperture A. Then its area A' visible from aperture A is roughly $(2D \tan 8°)$ × $(2D \tan 35°)$ ≈ $0.2D^2$. The current setup has D = 120 cm. The visible area of the panel subtends $\Omega_1 = A'/(D-L)^2$ steradians from the front of the baffle, where L = 27.6 cm is the baffle length. Similarly aperture A subtends $\Omega_2 = A/D^2$ steradians for light scattered from the panel, where A now is the area of the aperture. The terminating panel should be as black as possible.

Consider first light scattering from the outside of vane 8, reaching the panel and scattering from there into aperture A. The light intensity through A by this external scattering path is

$$B_c = B_0 \; a_8 \; \eta_8 \frac{\Omega_1}{2\pi} \; \eta_2 \frac{\Omega_2}{2\pi} \approx 6 \times 10^{-7} a_8 \; \eta_8 \eta_2 B_0 A \quad , \tag{1}$$

where a_8 is the effective beam area illuminating the outside portion of the vane, $\eta_8 \approx 0.05$ is its reflectivity, η_2 is the reflectivity of the terminating panel, and B_0 is the brightness per square centimeter of the collimated incident light beam. To ensure full illumination, the light beam must be slightly wider than the projected width of the vane 8 opening. The effective illuminating beam area on the outside of vane 8, $a_8 = 2h\Delta \approx 3$ cm^2 is the height h of the illuminating beam in the Y-direction, times twice (one for each side of the beam) the umbral width of the beam ($\Delta \geq 0.1$ cm).

Similarly, consider light scattering from the vanes within the baffle, reaching the panel and again scattering into A. Here

$$B_i = B_0 \; fA_8 \cos\theta \; \eta_{mb} \frac{\Omega_v}{2\pi} \; \eta_2 \frac{\Omega_2}{2\pi} \approx 5 \times 10^{-7} \; fA_8 \cos\theta \; \eta_{mb} \eta_2 \; B_0 A \quad , \tag{2}$$

where $f(\theta)$ is the average fraction of the light beam falling onto internal vanes that can be seen

16

by the panel. A_8 = hw, the height (h=15 cm) of the beam times the width (w = 11 cm) of the vane 8 opening. f varies from zero at $\theta = 90°$, to near unity at $\theta = 0°$. Typically $fA_8 = 75$ cm^2. Here $\eta_{mb} = 0.005$ is the reflectivity of Martin Black and $\Omega_v = A'/(D-L+d)^2 \approx 0.85\ \Omega_1$ for light coming from depth d within the baffle behind vane 8.

When baffle, photomultiplier, and terminating panel are all enclosed within a dark box, and entering light is collimated where it enters the box through one of the side walls, then light scattering *once* inside the box and then reaching the terminating panel is reduced by a factor of order $\eta_{box}\Omega_1/(2\pi)$. This factor is sufficiently small in our setup to render more than one in-box scattering (the one off the terminating panel) negligible. Then the total externally scattered light contribution to the light-rejection measurement is

$$R_c = \frac{B_c + B_i}{B_0 A} = 6\times10^{-7} a_8 \cos\theta_8 \eta_8 \eta_2 + 5\times10^{-7} fA_8 \cos\theta \eta_{mb}\eta_2 \approx 2.8\times10^{-7}\cos\theta \eta_2 \ , \qquad (3)$$

where the right-hand side employs the above values for a_8, η_8, fA_8, and η_{mb}. Contributions from eq(1) and eq(2) are comparable. In order to measure the baffle down to the SMEI specification requires that $R_* < 10^{-10}$. The choice of black velvet for the surface of the terminating panel yields η_2 of order 1-2$\times10^{-3}$, which does not satisfy this condition except for large θ, but comes close. We note when D >> L (nearly true here) $R_* \propto D^{-4}$, which means only a 10% increase in size of the box (and hence distance to the terminating panel) should yield a 40% improvement. The present box size was dictated by available laboratory space in our previous building, although it *is* about as large as we can handle, given that box, baffle and light detector are one rigid unit to be manipulated by chainfall and large horizontal bearing, for adjusting orientation relative to the light source.

III.   SCATTERING INTRINSIC TO THE VIEWING COLUMN

Fundamental limits to the technique illustrated in figure 1 arise when the measurement does not take place in an evacuated chamber. As seen in figure 1, the illuminating light column passes through the pyramidal column viewed by the aperture, and light from it can be directly scattered into aperture A either by air molecules (Raleigh scattering) or by water and dust particles suspended in the air (Mie scattering). This section evaluates these sources of spurious stray light.

A. RALEIGH SCATTERING

The Raleigh scattering cross section is (see e.g. Measures 1984 or Coulson 1988)

$$\frac{d\sigma}{d\Omega} = \frac{\pi^2(n^2-1)^2}{N^2\lambda^4}\ [\cos^2\phi\cos^2\theta + \sin^2\phi] \qquad , \qquad (4)$$

17

where n is air's refractive index, Loschmidt's number N is derived from Avogadro's number by

$$N = \frac{6.025 \times 10^{23}}{22,400} = 2.69 \times 10^{19} \quad , \tag{5}$$

λ is the light wavelength, θ is the scattering angle, and ϕ is the angle between the scattering plane and the linear polarization of the incident light. Evaluating the factor in front of the angular terms in eq(4) with $(n-1) = 2.76 \times 10^{-4}$, and $\lambda = 6.3 \times 10^{-5}$ (red laser light) yields 2.6×10^{-28} cm^2 ster^{-1}. The amount of this scattered light intercepted by aperture A is derived from eq(4):

$$\frac{B_{Ray}}{B_0 A} = \frac{d\sigma}{d\Omega} NV \frac{\Omega_A}{A} \approx 7 \times 10^{-9} \frac{h w^2 [\cos^2\phi \cos^2\theta + \sin^2\phi]}{2 \tan\theta L^2} = 8 \times 10^{-9} [\frac{\cos^2\phi \cos^2\theta + \sin^2\phi}{\tan\theta}], \tag{6}$$

where $V = hw^2/(2\tan\theta)$ is the illuminated volume and, $\Omega_A \approx A/L^2$ is the solid angle subtended by aperture A from the illuminated volume.

The final coefficient of eq(6) is about 100 times larger than it should be for this process to be ignored in the present method; furthermore, eq(6) presents only a lower bound to the amount of scattered light since more than just air molecules contribute. However, this scattering is a highly polarized process. Consider first the polarization of the incoming light. Eqs(4) and (6) reach minima at both $\phi = 0°$ and $90°$, but the reduction is always more for $\phi = 0°$, except at $\theta = 0°$ where polarization doesn't matter and eq(6) has diverged anyway. Let the incident beam be polarized in the scattering plane such that $\phi = 0°$. Then eq(6) becomes

$$R_r = \frac{B_{Ray}^{\phi-0}}{B_0 A} = 8 \times 10^{-9} [\frac{\cos^3\theta}{\sin\theta}] \quad . \tag{7}$$

Eq(7) is nonzero except at $\theta = 90°$. Since *this* scattered light remains polarized in the scattering plane ($\phi_2 = 90°$), it can be reduced by placing a polarizer in front of the light detector. If each polarizer's extinction for perpendicularly polarized light is better than 0.5%, then the contribution to the baffle light-rejection measurement from Raleigh scattering in air is below $R_r < 10^{-10}$ over the entire range $20° < \theta < 90°$ of interest for SMEI. The key question, of course, is how much better than this the polarizers must be to control also contributions from dust and water, and the extent to which scattering from larger dust particles depolarizes the light.

B: MIE SCATTERING

The above treatment does not include contributions from water vapor, small water droplets and airborne dust, which add more background light. This is "Mie scattering" which, for particle

18

size $\delta < \lambda/\pi$, has similar angular and polarization properties to the Raleigh process (McCartney 1976; Measures 1984; Coulson 1988). This adds typically 3 to 10 times more than Raleigh scattering (Diermendjian 1964). For larger δ the angular distribution favors forward scattering, a hallmark of the Mie process. Mie calculations assume homogeneous spherical particles while airborne dust particles are highly irregular in shape, increasingly so as they get large. As a result, Mie theory serves here mostly as a general guide.

C. LABORATORY MEASUREMENTS

Figure 2 shows the setup used to measure Raleigh and dust-particle scattering. The CCD camera is a photometer focussed on the beam of laser light illuminating the air; the CCD also resolves larger individual illuminated particles. The light source is a 5 milliwatt He-Ne laser. The camera lens has 5.2 cm focal length and is focussed 64 cm in front of the lens assembly where the laser beam crosses the optical axis. The lens opening is f2.8, and thus subtends $\Omega = 6 \times 10^{-4}$ steradians from the object plane. In 100 seconds, a direct laser exposure would have $B_0 \approx 10^{15}$ analog-to-digital units (ADU's) of CCD response. Expected Raleigh-scattered-light brightness per centimeter is given by eq(4), multiplied by $(B_0 N\Omega/\sin\theta)$. Evaluating at $\theta = 90°$ for unpolarized incident light ($< \sin^2 \phi > = \frac{1}{2}$) predicts about 2200 ADU's per cm for this exposure time.

Polarizers select ϕ_1 and ϕ_2, polarization respectively of incident and detected light. The CCD field of view covers 8 cm of laser beam for scattering-angle $\theta = 90°$. Scattered-light brightness per centimeter of projected laser-light path is given by the sum of brightness excess over background, within a band of 10×35 pixels, corresponding to 0.3×1.0 cm in the object plane. Actual performance is also governed by the quality of the polarizers: transmission of polarized light through the photographic filters used here varies between about 75% and 4% as Φ varies from 0° to 90° relative to ϕ.

1. CLEAN ROOM

Initial measurements took place within a laminar-flow, HEPA filtered work station located in a clean room facility. HEPA filters remove particles with $\delta > 0.3\mu$: here scattering contributions come from Raleigh, and from Mie for water and dust with $\delta < 0.3\mu$. Figures 3 and 4 show the results. Angular distributions are as expected for Raleigh alone, but amplitudes are between double and triple those expected from eq (4). If the SMEI baffle measurements were to take place in this environment, the crossed-polarizer extinction would have to be about 20 times better than that for the filters used in the present measurements.

The enhancement over Raleigh of figures 3 and 4 is not unreasonable considering the aerosol particle counts described by Deirmendjian (1964): of order m = 100 particles per cubic centimeter in this size range. Evaluating

$$B = B_0 \, m \, \frac{\pi\delta^2}{4} \, \frac{\Omega}{4\pi} \qquad (8)$$
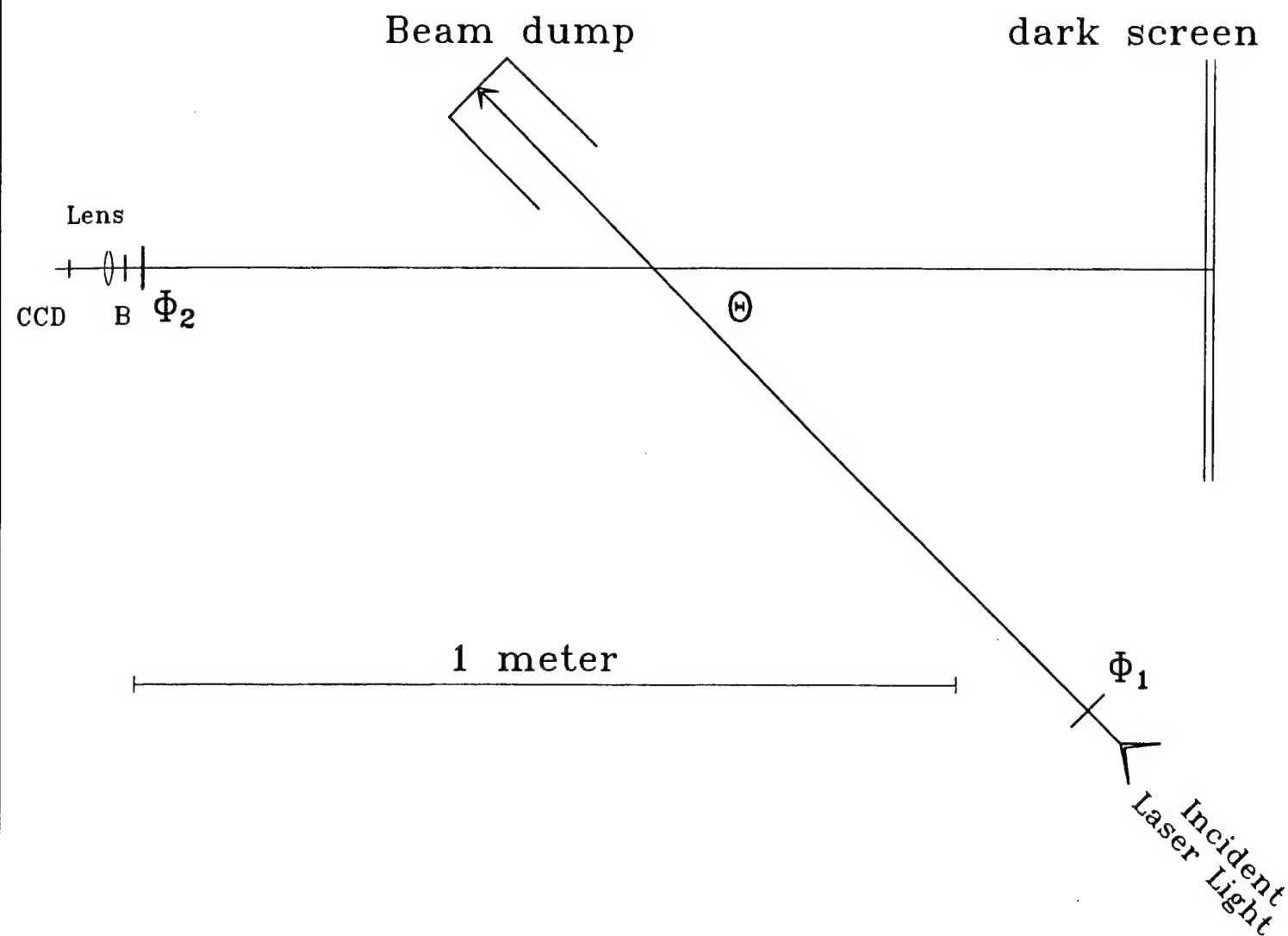
Figure 2. Polarized-light scattering measurement setup. Incident laser light (lower right) crosses the optical axis (center) and enters the beam dump, which absorbs it. The CCD-lens assembly (left) views the dark panel and the laser light scattered by the air. An IR cutoff filter "B" limits the CCD viewing to $\lambda < 0.7\mu$, and polarizers Φ_1 and Φ_2 select the polarization respectively of the incident light beam and the detected light.

Figure 3. Single-polarizer results

Figure 4. Double-polarizer results.

with the above values for B_0, δ, and Ω yields 3375 additional ADU's, which is about what we see. A more accurate calculation of expected Mie scattering in this setup would require much more detailed information than we presently have about particle numbers and properties (see e.g. chapter 5 in McCartney 1976), and is probably not required at present.
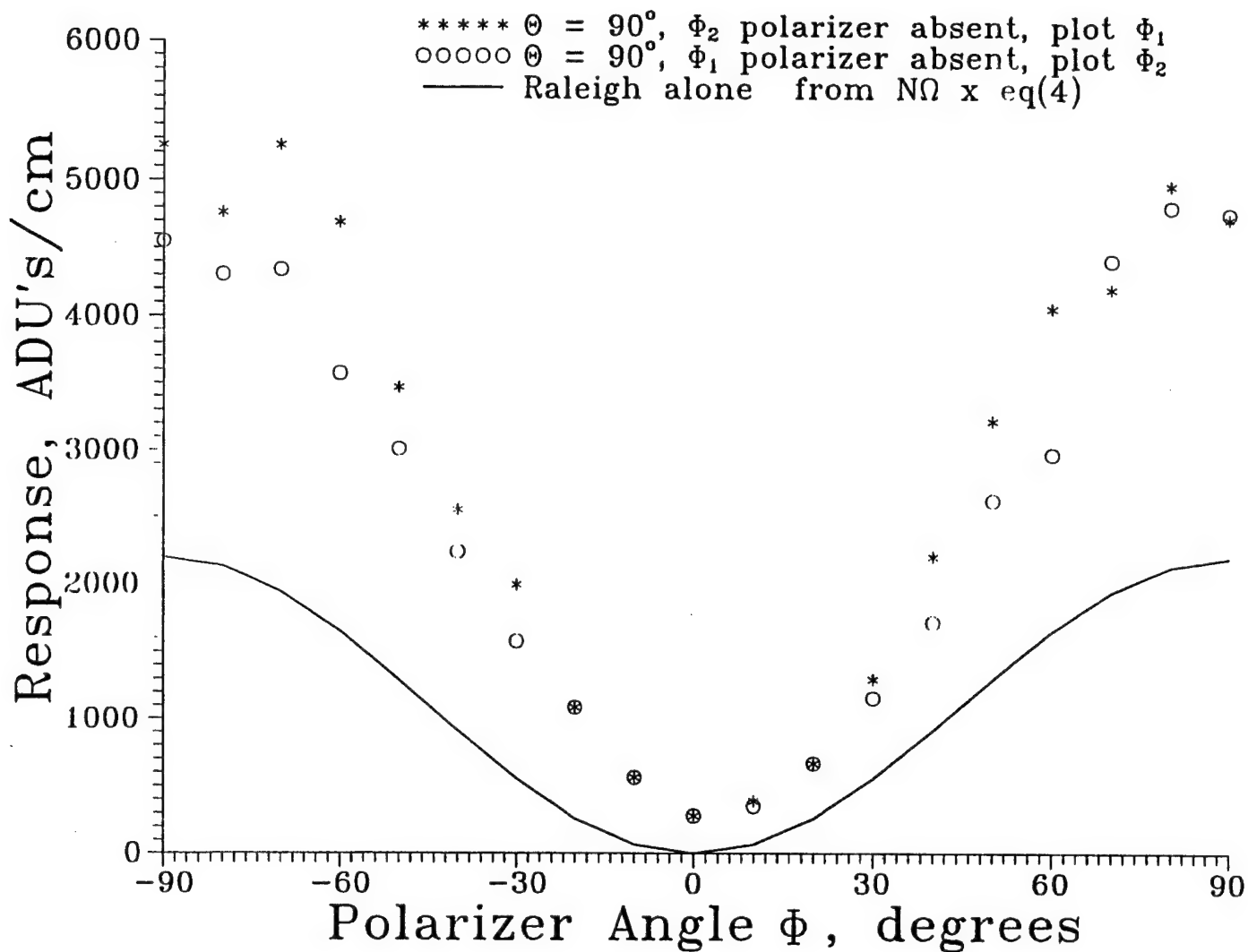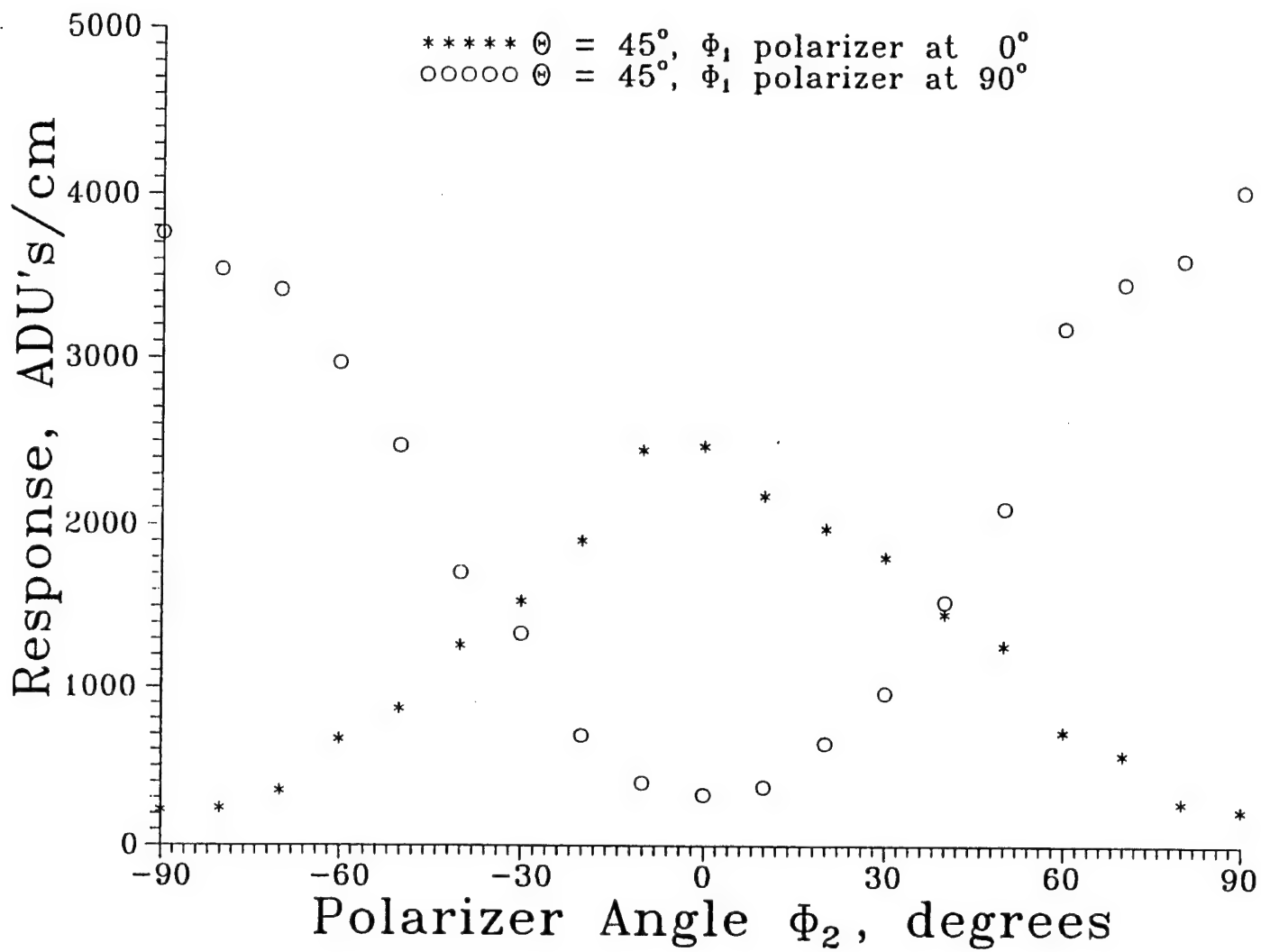
2. LABORATORY

The baffle measurements are more conveniently made in a laboratory environment, since the velvet lining the test box is unpopular in clean rooms. However, this convenience brings more dust and a larger Mie contribution. Since laboratory dust particles are bigger, some depolarization may occur in the scattering, even further degrading the performance of this technique.

The setup of figure 2 was moved to the velvet-lined box at $\theta = 90°$. The box was undisturbed for two weeks, its fans circulating air through a conventional paper filter. Polarizer Φ_2 was removed and the $\Phi_1 = 0$ and $90°$ ("*" in figure 3) points measured. These had increased respectively, from {280, 5000} to {525, 5600} ADUs. Next the fans were shut off and doors removed to admit air and dust from the room. The values became {580, 6825}. Observing with $\Phi_1 = 0$ and $\Phi_2 = 90°$ the light distribution along the laser beam became very irregular, with bright spots marking locations of various particles illuminated by the laser light. These were absent in the clean room, where the residue was a barely detectable 70 ADUs. In the laboratory the minimum residue was about 250 ADUs, and this increased to 1000 ADUs when typical bright particles were included.

IV. DISCUSSION

The method illustrated in figure 1 can deliver the desired 10^{-10} ratio relative to direct illumination of aperture A, over the range $20 < \theta < 90°$, provided the incident light beam is polarized in the plane of figure 1, and a second polarizer behind A is set for out-of-the plane polarization. Rejection of polarized light at $90°$ should be better than 10^{-3}, about a decade beyond the photographic polarizers used for the measurements presented here. Higher quality polarizers from several catalogs advertise typically 4×10^{-4}, so this should not be a problem. Testing the baffle with polarized light is a complication, since Martin Black's textured surface almost surely polarizes the light it scatters, with reflectivity which is also sensitive to incident polarization.

A clean room does not appear to be required for the success of these tests, but reaching full performance in the laboratory will require some attention to dust control. Including bright particles raised the noise threshold by a factor of four in the measurement above. If large dust is controlled, the impact of using the laboratory in place of the clean room appears to be only an insignificant 10-20% increase in the background level.

The scattering background of the previous section would be eliminated if the light beam illuminating the baffle interior were to avoid the viewing column. Thus, laser spots could be placed at selected locations on individual baffle vanes and septum bottoms, and light through A recorded. Probably all interior locations in the outermost two baffle septums could be explored

while avoiding the viewing column. This gets more difficult deeper in the baffle. The trouble with this technique is that it lacks the straightforward normalization of figure 1. However, once a prototype baffle is thoroughly tested and understood, this alternative method might well be adopted for the SMEI flight baffles, since the prototype evaluation implicitly includes normalization.

REFERENCES

Born, M., and Wolf, E., *Principles of Optics*, 6th (corrected) ed. (Pergamon, New York 1989).

Breault, R.P., "Problems and Technologies in Stray-Light Suppression," in *Stray-Light Problems in Optical Systems*, SPIE proceedings 107, 2-23 (1977).

Coulson, K.L., *Polarization and Intensity of Light in the Atmosphere*, (A. Deepak Publishing, Hampton, VA 1988).

Deirmendjian, D., "Scattering and Polarization Properties of Water Clouds and Hazes in the Visible and Infrared," *Applied Optics* 3, 187-193 (1964).

McCartney, E.J., *Optics of the Atmosphere - Scattering by Molecules and Particles*, (Wiley, New York 1976).

Measures, R.M., *Laser Remote Sensing - Fundamentals and Applications*, Wiley, New York 1984).

Pompea, S.M., and McCall, S.H.C.P., "Outline of Selection Processes for Black Baffle Surfaces in Optical Systems," in *Stray Radiation in Optical Systems II*, SPIE proceedings 1753, 92-104 (1992).

Appendix III

Dust Control Needs for SMEI

DUST CONTROL NEEDS FOR SMEI

Andrew Buffington
Center for Astrophysics and Space Sciences
University of California, San Diego
La Jolla, CA 92093-0424

April 27, 1998, revised 22 May 1998

I.   INTRODUCTION

Dust collecting on SMEI optical surfaces may degrade its performance to the point where the 0.1% differential photometry specification is compromised. Furthermore, dust may come loose during launch vibrations and be illuminated by sunlight during spacecraft maneuvers throughout the mission, as it floats around in the front sections of the baffle. Finally, dust may settle on the CCD, partially covering the surface and thus contributing to the "subpixel gradient error budget". This memo investigates expected dust-deposition rates during the ground-preparation stage of SMEI and suggests handling procedures to control the impact of dust on optical performance.

II.   ATMOSPHERIC DUST MODELS

"Dust" here means airborne particles of characteristic size δ between about 0.1 and 100μ. Any particular clean room, home or laboratory has a suspended-dust number distribution $n(\delta)$ that is determined by the dust-source-function feeding it and velocity $v(\delta)$, the rate at which particles settle under gravity. Within the above range of δ, $v(\delta)$ can be approximated (e.g. see Bolz and Tuve 1970 for spherical particles of density 2 g cm^{-3}) is

$$v(\delta) = 0.007 \ \epsilon \ \delta^2 \quad , \tag{1}$$

where v is in cm s^{-1}, δ is in microns, and $\epsilon \approx 0.1$ accounts for nonspherical particles.

Various forms of $n(\delta)$ are encountered in the literature. Deirmendjian (1964) uses $n(\delta) \propto \delta^{-4}$ for "continental hazes", and $n(\delta) \propto \delta e^{-6.324\sqrt{\delta}}$ for "Los Angeles aerosols". The latter has relatively more smoke particles ($\delta \approx 1$) and less sea salt dust ($\delta < 1$), construction dust, danders and pollens ($\delta \gg 1$).

The Federal clean-room standard (e.g. Dorman 1974, page 511) defines the "Class" of a clean room as the number of particles per cubic foot having $\delta > 0.5$:

$$N_{clean \ room \ class} \equiv N_{c.r.c.} = \int_{0.5\mu}^{\delta_{max}} n(\delta) \ d\delta \quad . \tag{2}$$

Urban households with open windows and doors typically have $N_{a.r.a.} = 10^6$ to 10^5, while closed, air-conditioned rooms are typically 10^5 to 10^4, and appropriately sealed clean rooms with good air circulation and HEPA filters are 10^3 to 10^2. Well maintained work-station hoods with low traffic get down to 10 or even 1. Moreover the permitted contamination levels for larger particles, $\delta > 0.5$, must lie below

$$N(\delta) < N_{a.r.a.} \ (\frac{\delta}{0.5})^{-2.15} \quad . \tag{3}$$

Thus in effect, the clean room specification yields:

$$n(\delta) \equiv \frac{dN(\delta)}{d\delta} = 2\times2.15 \ N_{a.r.a.} \ (\frac{\delta}{0.5})^{-3.15} = 0.48 \ N_{a.r.a.} \ \delta^{-3.15} \quad . \tag{4}$$

Eq(4) lies midway between Deirmendjian's two cases and probably represents a typical particle distribution shape for an indoors, air-conditioned environment.

Converting eq(4) to n′ = particle number per cubic centimeter per micron in size yields

$$n'(\delta) = 1.7\times10^{-5} \ N_{a.r.a.} \ \delta^{-3.15} \quad . \tag{5}$$

For some calculations δ_{max}, the largest size of airborne particles in a room, is important. In the absence of local sources of large particles (hairs and clothes fibers) δ_{max} may simply be the cutoff set by the largest hole in a house's screens or in a room's air-conditioning system. It could also be smaller, since $v(\delta)$ increases rapidly with δ and $n(\delta)$ drops rapidly when particles fall from the air stream before they can make it through the air-supply duct. With $v = 50$ cm s^{-1}, the value $\delta_{max} = 100\mu$ used in the indoor context here is probably conservatively large. Even in non-air-conditioned urban homes, one hardly ever finds individual dust particles as large as a millimeter, generated at construction sites and elsewhere, unless they are "tracked in". These stand little chance of arriving by air, having long since fallen to the ground close to where they were made. Once settled on the ground, it takes a stiff wind to make them airborne again. The clean-room literature contains little discussion of the parameter ϵ, the "eccentricity" of the dust particles. This parameter is important in the settling velocity and also in determining whether particles become airborne again. Presumably ϵ varies greatly with location and type of contaminant: we will return to this issue in the final section of this memo. In this memo we use ϵ loosely, employing it in eq(1) as the ratio of actual-particle mass to that of an equal-area sphere having diameter δ and density 2, but in following sections also to provide the effective optical area ($\epsilon\delta^2$), of a non-spherical particle whose largest dimension is δ.

III. PARTICLE DEPOSITION AND OPTICS CONTAMINATION RATES

An area dA perpendicular to the direction of the settling-out velocity vector (usually a horizontal area) accumulates particles at the rate

$$\frac{d^2n}{dA\,dt} = \int_{\delta_{min}}^{\delta_{max}} v(\delta)\,n'(\delta)\,d\delta \approx 1.2 \times 10^{-7}\,\epsilon\,N_{a.r.c.} \int_{\delta_{min}}^{\delta_{max}} \delta^{-1.15}\,d\delta \quad , \qquad (6)$$

where on the right-hand side we have utilized eqs(1) and (5). The integral on the right-hand side of eq(6) is close to logarithmic, but a small negative power of integrand remains and thus somewhat more particles are deposited in logarithmic intervals at small δ than those at large δ.

The optical impact of particle deposition is proportional to particle area, which we here take to be approximately $\epsilon\,\delta^2$. Thus the initial rate df/dt at which a unit area becomes fractionally obscured by particles is given by

$$\frac{df}{dt} = \int_{\delta_{min}}^{\delta_{max}} \epsilon\delta^2\,v(\delta)\,n'(\delta)\,d\delta \approx 1.2 \times 10^{-15}\,\epsilon\,N_{a.r.c.} \int_{\delta_{min}}^{\delta_{max}} \delta^{0.85}\,d\delta \quad , \qquad (7)$$

where the right-hand side has a factor of 10^{-8} to convert square microns to square centimeters. This equation shows that the large-particle cutoff δ_{max} predominates in the fractional areal coverage, i.e., the few largest particles deposited dominate the obscuration. The lower limit of integration δ_{min} is insignificant in calculating obscuration, and of minor importance even in calculating numbers of particles deposited in eq(6).

Eq(7) is only the initial rate at which area becomes covered: as the dust builds up, the fractional uncovered area f diminishes exponentially, and eq(7) diminishes proportional to f. Eq(7) confirms common experience, that even the dustiest places in the home take months to become covered so completely as to obscure the view underneath. Thus, with $N_{a.r.c.} = 10^6$, $\delta_{max} = 100\mu$, and $\epsilon = 0.1$, df/dt must be integrated for over a month for the integral to approach unity.

IV. OPTICAL IMPACT UPON SMEI

The design parameters to choose here are the environment $N_{a.r.c.}$, and the duration τ over which eq(7) is integrated. The "Dust Dose" is proportional to $N_{a.r.c.}\tau$. If SMEI optics and baffle are left open during most of integration and test, τ is the several months to a year it takes to accomplish these. However, if the optics and baffle openings are covered during most of the time when not in use, the effective τ is reduced and a significantly larger $N_{a.r.c.}$ can be tolerated, which in turn yields savings in time and trouble.

A. BAFFLE INTERIOR

The baffle interior reflectivity after treatment with Martin Black is $\eta \approx 0.5\%$. The reflectivity may increase 100-fold in locations covered by dust. The baffle's front vane opening is about 500 cm^2, while the blackened interior area is about ten times this. Assume a worst case for the moment: the entire baffle interior area is exposed, with dust settling equally on all surfaces. Light reaching the aperture scatters typically 3-4 times within the baffle. Thus, in this case baffle performance worsens roughly $\propto \eta^{3.5}$, so 1% of baffle area covered with dust increases stray light passing through about tenfold, which is clearly unacceptable. However, with only 0.1% of the area covered, stray-light growth is only 40%, acceptable.

Evaluating eq(7) with the above 0.1% goal for $\int df/dt$ yields $\epsilon\, N_{a.r.c.}\,\tau \leq 3\text{x}10^8$. This means that the SMEI baffle components can be exposed within a Class 10,000 environment with $\epsilon = 0.1$ for 3 to 4 days before 0.1% of their area becomes obscured, and thus yield the above baffle performance degradation. Once assembled, the baffles become less vulnerable since the effective opening entrance to dust is tenfold reduced. An allowable exposure time probably is several months when including the facts that the baffle opening is usually vertical, and larger particles tend to deposit out toward the front.

Once a baffle is assembled, common sense suggests that its front cover should be kept closed except during optics tests requiring that it be open. Probably most of the time the baffle can also be bagged. With these precautions in place, probably a laboratory environment ($N_{a.r.c.} < 10^5$) with minimal traffic will prove satisfactory for most of the SMEI integration and test work. Moreover, baffles and probably an entire SMEI camera assembly can simply be covered and bagged for shipment, and does not require further dust-control measures. With these precautions, dust on the baffle surfaces will have collected primarily during the initial baffle assembly, and not much more during subsequent activities.

B. LOOSE PARTICLES IN FLIGHT - - FRIGHTENING FLOATERS

Some particles accumulated within the baffle during SMEI ground preparation will shake loose during launch vibrations. Although the venting gas carries away many of these, others remain to be jarred loose after the gas has vented, and yet more from time to time by station-keeping accelerations and operation of the SMEI shutter. These float back and forth through the viewing column until they either reattach or wander out the front aperture. SMEI data within the hemisphere towards the sun is significantly impacted by sunlight directly illuminating these "floaters".

A particle with albedo η at distance z from the SMEI aperture A illuminated by the sun has an apparent brightness of

$$B = \frac{\epsilon\delta^2}{A}\,\eta\,\frac{\Omega}{4\pi} \times 10^{15} = \frac{\epsilon\eta\delta^2}{4\pi z^2} \times 10^7 \approx 30\delta^2 \qquad (8)$$

in S-10 units, spread over an out-of-focus patch covering several 1° sky bins in the field of view. The right-hand side of eq(8) takes $\eta = 0.35$, $\epsilon = 0.1$ and $z = 30$. As before, δ is in units of microns, and here the aperture subtends $\Omega = A/z^2$.

Eq(8) shows that illuminated floaters are a serious matter for SMEI data analysis. Even the smallest 0.1μ particle yields about 0.3 of one S-10, the SMEI accuracy specification. Thus, nearly the entire size range of dust gathered on baffle surfaces can cause significant trouble when loose and illuminated. When a bright illuminated floater occurs, we must remove that piece of sky from the data analysis. Clarence Korendyke reports that in SOHO, dielectric attraction to anodized walls strongly retains particles having $\delta < 5\mu$. Presumably particles with small ϵ bind more strongly. The key question: how many larger loose particles will be illuminated within a given single SMEI camera data frame? The 0.1% coverage of the previous section deposits about 70 particles cm^{-2} with $\delta > 5\mu$, and thus about 3×10^5 particles overall. To avoid the above trouble, only a tiny fraction of these can be loose at any given time. Probably only a few do come loose, but we don't know whether the fraction is as small as 10^{-6}. Since these particles eventually disappear out the front aperture, SMEI may cleanse itself as the mission progresses.

The baffle assembly operation will probably be done by hand, perhaps with the help of alignment jigs, and τ likely will be several hours per baffle. Thus $N_{c.r.c.}\tau$ will be 10^8 to 10^9 from this source depending on how good the clean room is. Controlling $N_{c.r.c.}$ with nearby human activity is difficult. With respect to floaters, we'll probably just have to be as careful as we can, without compromising necessary tasks to build and test the SMEI flight units, and hope for the best!

C. CCD AND OPTICS

Within the optics box the dust-sensitive places are the polished mirror surfaces and the exposed light-sensitive portion of the CCD. This latter will be kept cold, which may or may not attract dust particles and/or cause them to stick. As observed in the Introduction, dust on mirrors and particularly on the CCD can compromise the photometric performance of SMEI. Aperture A has only 1/300th the area of the baffle's front opening, so the quantity of baffle dust coming through A should be negligible given we weren't swamped by the "floaters" of the above section. Moreover, most of the interior of the strong box can be carefully cleaned at final assembly, and then closed up to avoid further dust exposure. Comparable care to that of other space-borne optics experiments should probably suffice here. The CCD should be warm during launch, to avoid attracting any of the dust that may be swept through the SMEI strong box as the gas vents from the baffle and electronics boxes.

V. MEASUREMENTS

"Witness plates" composed of Scotch transparent tape with a steel washer defining an area of 0.2 cm^2 were exposed in various places with the sticky side horizontal and facing up. Exposure was $\tau = 1.4 \times 10^6$ sec except for the "control" with 2.6×10^6 sec. As expected, the largest particles had $\delta \approx 100\mu$, except in the velvet box and "home". The velvet-box plate contained 4

particles with $\delta > 100\mu$, and "home" contained 18 hairs about 10μ in diameter and lengths varying from 100 to 1000μ. The value $\epsilon \approx 0.1$ used throughout this memo appears reasonable on average, although a smaller value would be better for large particles and a larger one for small particles.

The samples were next examined under a microscope and the particles counted. The following table presents results, together with two inferred values for $N_{c.r.c.}$ using $\epsilon \approx 0.1$, the first including particles between 10 and 100μ, the second using just those between 10 and 30μ.

TABLE: PARTICLE COUNTS AND INFERRED $N_{c.r.c.}$

LOCATION	Largest particle	$N > 30\mu$	$N > 10\mu$	$N_{c.r.c.}(10\text{-}100\mu)$	$N_{c.r.c.}(10\text{-}30\mu)$
Control (*)	50μ	1.6	7.5	1700	2200
Clean Room	100μ	2	6	1350	1800
Velvet Box	175μ	11	30	6700	8500
Laboratory	85μ	27	69	15000	20000
Home (**)	90μ	49	180	40000	60000

* Particle counts reduced here to equalize exposure time
** Excluding 18 large hairs

The results of this table are about as expected considering that several contamination particles probably were added while preparing the tape samples and/or while examining them under the microscope. The higher value for $N_{c.r.c.}$ using only the smaller size particles (final column above) provides further evidence for a particle-size cutoff at about $\delta = 100\mu$. The improvement of the velvet box over the laboratory can be attributed to its fan-and-filter system, which maintained a small overpressure inside during the exposure, but probably also swept larger particles off of the velvet and kept them circulating. Laboratory and velvet-box values of $N_{c.r.c.}$ are about as expected from direct observation of illuminated circulating particles using our CCD camera.

REFERENCES

Bolz, R.E., and Tuve, G.L., "Handbook of tables for Applied Engineering Science", Chemical Rubber Co., Cleveland OH, 1970, page 547.

Deirmendjian, D., "Scattering and Polarization Properties of Water Clouds and Hazes in the Visible and Infrared", *Applied Optics* 3, 187-193 (1964).

Dorman, R.G., "Dust Control and Air Cleaning", Pergamon, New York, 1974.

Appendix IV

Stray-Light Rejection Results with the SMEI Prototype Baffle

STRAY-LIGHT REJECTION RESULTS WITH THE SMEI PROTOTYPE BAFFLE

Andrew Buffington
Center for Astrophysics and Space Sciences
University of California, San Diego
La Jolla, CA 92093-0424

October 16, 1998

I.   SUMMARY

A prototype baffle, described by B.V. Jackson in memos dated 1& 2 June 1992 and 9 March 1993, was constructed at the University of Birmingham, blackened at Lockheed-Martin, and delivered to UCSD in late July of this year. This memo describes measurements with this prototype. The main result (also incorporating our optics-box prototype evaluation): this baffle **will deliver** the 10^{-15} rejection relative to direct sunlight desired for SMEI, but with little safety margin. Further, the measurements show SMEI can also operate with elongation $10° < \epsilon < 20°$, but in this region has stray-light amounts ranging from comparable to, and up to 5 times larger than, typical transient heliospheric signals measured at the same ϵ.

II.   TEST SETUP & CLEAN ROOM

Measurements took place within a HEPA-filtered, laminar-flow workstation, as described in our 28 April 1998 memo. The baffle's outer cover was removed during measurements, a total of ~100 hours, with the front opening vertical most of the time. This procedure should render negligible the "dose" of dust particles gathered by the baffle (see our 27 April 1998 memo).

Light scattered from a Martin-Black surface largely retains its original polarization. Thus the crossed-polarizer method advanced earlier for removing viewing-column scattered light is impractical, since Raleigh- and baffle-scattered light are not thus distinguishable. Therefore the photomultiplier-detector method was abandoned in favor of a CCD camera viewing through the rear of the baffle and detecting light scattered from the interior vane structures. This imaging method directly distinguishes air-column-scattered light from baffle-scattered light, since the latter comes from the baffle structures and the former from the viewing column.

Figure 1 presents a schematic diagram of the baffle, labelling prominent features referred to in this memo. The CCD camera was placed immediately behind the aperture (Vane Z0). The 52 mm Nikkor AF lens supplied with the camera (memo dated 10 February 1993) and a similar 28 mm AF lens were used, both at f2.8, with +7 diopters of Tiffen close-up lenses and with an Edmund #53710 infrared cutoff filter to remove light having $\lambda > 0.7\mu$. This combination enables the camera to focus on the rear of vane Z3, typically ~10 cm from the lenses. The camera was angled about to explore most of Z3, viewing at least 1.2 x 1.7 cm with the 52 mm lens, and 2.2 x 3.2 cm with the other. The major results were confirmed with both lenses.
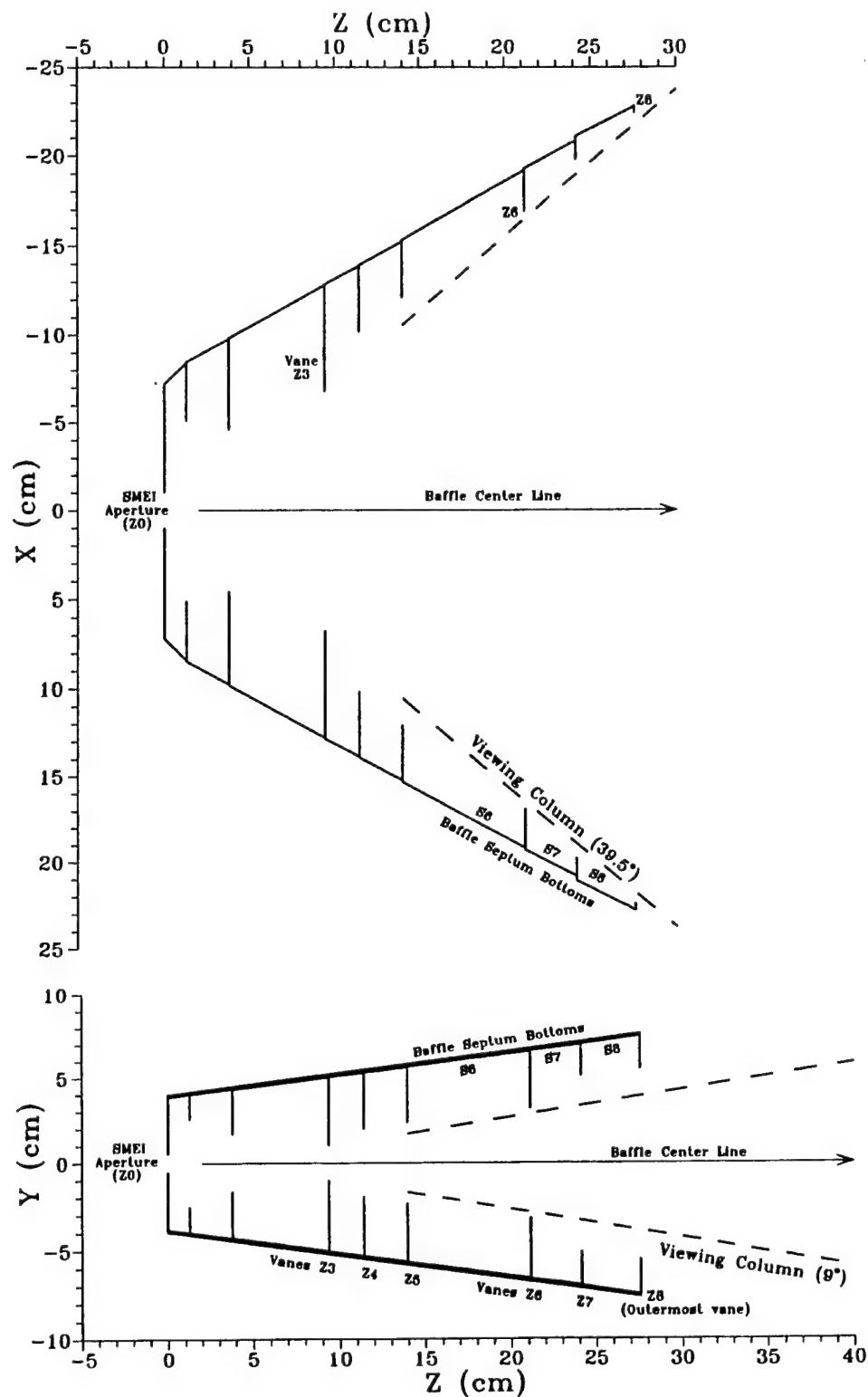
Figure 1. Schematic diagrams viewing from above and to the side of the SMEI baffle, showing the "critical vanes" Z3 and Z6, the main SMEI Aperture (Z0), and further vane and septum structures. Dashed lines mark the "Viewing Column", within which Raleigh scattering from the air and light from the room beyond is directly viewed through Z0.

The baffle was mounted within the HEPA work station, so as to view out into the room. Here most lines-of-sight within its field of view were terminated by two 100 x 112 cm black-velvet-covered styrofoam panels hung vertically at a distance of 170 cm from the rear of the baffle. These remained undisturbed and were separate from the laminar-flow air circulation of the work station, and thus did not pose a contamination hazard either to the baffle or the work-station filters. Fortunately, this "clean room" is not too clean and we are its only users to date, so no one has complained about the velvet or our frequent going in and out without frocking up and scrubbing down!

Most measurements described here employed a 5 mW Metrologic 0.633μ Neon-Helium laser having spot size 0.68 mm and 2 milliradians angular divergence. Three key measurements were confirmed using the broadband light source described in our 28 April 1998 memo. This had its brightness eightfold increased (to 3.5×10^{-4} of sunlight), by replacing its previous 20 W bulb-and-reflector with two 100 W halogen bulbs and an external reflector; this provides a 14 x 14 cm beam of parallel light, whose integrated CCD response is roughly twice that of the laser.

III. MARTIN BLACK REFLECTIVITY MEASUREMENTS & SMEI EXPECTATIONS

Reflectivities of several Martin Black samples and other materials were measured for both incident and outgoing laser light at 45° to the normal of the surface. A measurement within the baffle was made at a typical location on the front of vane Z3: recent Martin Black has reflectivity ~0.01. Martin Black samples made years ago in conjunction with an early prototype baffle have 0.005. Good-quality black velvet from two manufacturers has 0.001.

Jackson used 0.005 reflectivity in his 1992 calculation of baffle performance: the expected rejection of background sunlight relative to direct solar illumination was $R_b (\Theta_x, \Theta_y) \sim 10^{-10}$ for incident angles $[|\Theta_x|, |\Theta_y|] \geq [60°, 20°]$, and dropping below 10^{-12} for $|\Theta_y| > 50°$. Here (see figure 1) Θ_x is angle in the baffle's long dimension, and Θ_y in the narrow dimension. Since light thus transmitted scatters typically three times within the baffle, results should scale roughly as the cube of the Martin Black reflectivity. Therefore for this particular baffle, given its reflectivity is twice larger than previously assumed, we expect a decade or so worse performance: i.e., light rejection ranging from 10^{-9} to 10^{-11} for the angular domains above. This is about what is found here.

IV. BAFFLE-PERFORMANCE MEASUREMENT AND NORMALIZATION

Baffle performance is most simply evaluated by illuminating its entire front opening with parallel light having a solar spectrum and brightness per unit area B_0. A detector directly behind aperture Z0 measures the residue $r_b (\Theta_x, \Theta_y)$ of light passing through Z0, and baffle background-light rejection is then given by:

$$R_b (\Theta_x, \Theta_y) = r_b (\Theta_x, \Theta_y)/(B_0 A_{Z0}) , \tag{1}$$

where $A_{Z0} = 1.72$ cm^2 is the area of the SMEI aperture, the opening through vane Z0. Thus, r_b is normalized to R_b, dividing by the amount of perpendicularly incident light through Z0.

Evaluation of SMEI end-to-end performance follows this light residue through subsequent optics where most of it is absorbed upon the dark interior of the optics box, but a final residue r_{tot} lies within the $\Omega_{FOV} \approx 200$ square degrees SMEI field of view (FOV). The fundamental SMEI specification is then (for $[|\Theta_x|, |\Theta_y|] \geq [60°, 20°]$):

$$R_{tot}(\Theta_x, \Theta_y) = r_{tot}(\Theta_x, \Theta_y)/(B_0 A_{Z0} \Omega_{FOV}) \leq 10^{-15} . \qquad (2)$$

Given further that total solar brightness is $\sim 10^{15}$ S10 units (one S10 is the equivalent brightness of a 10th magnitude star per square degree), eq(2) specifies that background-light contamination of each sky bin within the SMEI FOV is less than one S10.

We have long considered direct laboratory measurement of $r_{tot}(\Theta_x, \Theta_y)$ unfeasible, given practical values of B_0 and of signal-to-noise ratios in CCD cameras. Instead, we plan to combine separate measurement of R_{optics}, the light-rejection of the optics box, with the R_b presented here, so $R_{tot} = R_{optics} \times R_b$. A final R_{optics} determination awaits manufacture and testing of flight-quality diamond-turned mirrors, but we have preliminary results using conventionally polished mirrors. Briefly, where $[\theta_x, \theta_y]$ are the angles equivalent to $[\Theta_x, \Theta_y]$ but where background light passes through the SMEI aperture Z0, $R_{optics}(\theta_x, \theta_y) \leq 10^{-6}$ for $[\theta_x, \theta_y] \geq [40°, 10°]$.

Restricting $[\theta_x, \theta_y] \leq [40°, 10°]$ limits background-light emission to within a band about a centimeter wide around the opening in, and upon the rear surface of vane Z3. Wider-angle light passing through Z0 stands little chance of making a major background-light contribution. (In principle, if this wide-angle light were >10 times more than from the rear of Z3, it could overwhelm the optics-box defenses: no evidence suggests that it is.) Thus, a measurement of R_b can exclude the wide-angle light and still be valid for simple multiplication with R_{optics} to yield R_{tot}. This allows using a CCD camera whose lens aperture covers this reduced range in $[\theta_x, \theta_y]$, compared with the photomultiplier which would have included $\theta \leq 70°$. By imaging Z3, the camera in turn separates viewing-column light (Raleigh scattering plus stray light from the velvet panels) from true background light, which now is viewed coming from the band around the opening in vane Z3. Observed intensities on the Z3 edge and its nearby rear surface must be appropriately scaled to account for the limited Z3 area coverage that the camera provides with either lens. The CCD camera views respectively about 2 or 7 cm^2 of the rear of vane Z3 for the 52 and the 28 mm lenses; the above Z3 band covers ~ 36 cm^2. Although the 28 mm lens views a larger area of Z3, its aperture covers typically only 1/3 the area of the Z0 aperture, so its readings require a further scaling correction.

A.   LASER MEASUREMENTS AND NORMALIZATION

When directly illuminating the CCD (determined using a suitable array of neutral-density filters to keep response from saturating) the laser produces $B_{laser} = 1.4 \times 10^{15}$ analog-to-digital units

(ADUs) in a typical 100 second exposure. For this camera, an ADU is ~70 electrons; a higher-gain setting used for some of the measurements reduces this to 17 electrons.

Because the laser beam is much smaller than the SMEI entrance aperture, eq(1) can no longer determine R_b. A single laser measurement consists of depositing the beam at some location i within the baffle and measuring r_i, the resulting illumination on Z3 visible through Z0. Consider that the baffle interior is divided into ($1 \leq i \leq n$) distinct regions over which this illumination r_i is roughly constant. Then R_b is given by:

$$R_b(\Theta_x, \Theta_y) = \sum_{i=1}^{n} \frac{r_i(\Theta_x, \Theta_y) \, A_i(\Theta_x, \Theta_y)}{B_{laser} \, A_{Z0}} \, , \qquad (3)$$

where A_i is the projected area of that region ($\perp$ to the incident beam) and the sum over i covers all illuminated baffle regions. For laser data then, the sum for $R_b(\Theta_x, \Theta_y)$ combines measured r_i for each region of the baffle illuminated at a given [Θ_x, Θ_y] with its appropriate calculated A_i.

B.   WHITE-LIGHT SOURCE

The white-light source not only covers a range of wavelengths but also is a spatially extended beam illuminating many baffle regions at once. We can think of it as implicitly measuring each r_i multiplied by its associated A_i, thus forming the eq(3) sum all in a single measurement. That's why eq(1) above is "simple": it directly yields R_b from a single r_b measurement. Our light source has $B_0 = 1.4 \times 10^{13}$ ADUs cm^{-2} in a 100s CCD exposure. Since the 14 x 14 cm beam rarely covers the entire aperture, two or sometimes three spatially translated readings are added to yield the final r_b. Unfortunately, this light source is not bright enough to produce a measurable diffuse illumination on the rear of Z3, unless $\Theta_x < 58°$ or $\Theta_y < 20°$ which allows light to directly illuminate through the opening in Z3. Therefore the detailed characterization of baffle performance employs laser measurements with eq(3), and the white-light source was used only to check these results at three incident angles.

V.   SCATTERING FROM VANE EDGES Z4 → Z6, PLUS Z3 DIFFRACTION

A bright-line edge appears on Vane Z3 when the laser illuminates vane edges on Z4 → Z6. The brightest case occurs when Z6 is illuminated at X = 0 (see fig. 1) and the CCD camera views the Z3 edge nearest to it: r_i = 500,000 ADUs from a centimeter-long region along the Z3 edge, 4×10^{-10} of the incident light. The bright region moves up or down along Z3 as the illuminated point is moved up or down along Z6. The laser-illuminated line-edges are very speckled and measurements vary by typically a factor of two as the camera or laser are repositioned. Viewing through Z0, Z3 blocks a direct view of Z6: on Z3 the amount of blocking varies from 1.2 to 7 mm as the viewpoint moves across Z0. At the minimum 1.2 mm, light needs a further deflection of only 1.45° at Z3 to gain potential access to the Z0 aperture.

Diffraction at the Z3 edge provides the deflection of this background-light source. The

bright line appears as expected for this virtual source: its apparent length is proportional to the camera-aperture width, while the length of a real scattering source is independent of this. Intensity is about as expected, given a 1% Z6 vane-edge reflectivity, roughly isotropic scattering of the residue, Z0's subtended solid angle, and the 6×10^{-4} diffraction intensity reduction appropriate here. Putting $A_{Z6} = 2.2$ cm^2 (Z6 vane height × laser-beam width) into eq(3) yields $R_{Z6} = 4.6\times10^{-10}$.

Similar measurements but with the Z5 or Z4 vane edges illuminated yield respectively $r_{Z5} \approx 100,000$ and $r_{Z4} \approx 20,000$ ADU's: these are at larger diffraction angles than Z6 and are thus reduced relative to it. Eq(3) and the appropriate vane areas (1.6 and 1.4 cm^2 respectively) here yield $R_{Z5} = 6.8\times10^{-11}$, and $R_{Z4} = 1.2\times10^{-11}$. This light's strong anisotropy favors further light rejection in the optics box, in effect reducing these R's tenfold compared with real illumination and isotropic scattering at Z3's edge.

VI.   SCATTERING FROM VANE EDGES Z4, Z5, and Z6, PLUS Z3 SCATTERING

Real scattering from the opposite-side Z3 vane edge is also observed here. Light passing through Z0 for Z6, 5, and 4 vane-edges respectively illuminated is 130,000, 70,000, and 40,000 ADUs. These values are consistent with estimates assuming two 1% vane-edge reflectivities, isotropic scattering, and appropriate solid angles for each. Associated eq(3) values are $R_{Z6} = 1.2\times10^{-10}$, $R_{Z5} = 4.7\times10^{-11}$, and $R_{Z4} = 2.3\times10^{-11}$. Because this light is uniform over the Z0 aperture, this mechanism dominates diffraction in determining end-to-end   performance R_{tot}. The two mechanisms are comparable for the Z6 contribution.

VII.   SCATTERING FROM SEPTUM BOTTOMS S6, S7, and S8

In the baffle's narrow cross-section (see figure 1), the placement of the "non-critical vanes" prevents the Z3 opening from directly viewing septum bottoms further out towards the open end of the baffle, that can be directly illuminated through its front opening. By adding one more reflection to legitimate light paths making their way through Z0, these secondary vanes enable the roughly 100-fold performance improvement this baffle should have, compared with its predecessor. However, this criterion is not satisfied in the baffle's wide cross-section, where incident light can scatter once and then pass through the Z3 opening. Once past Z3, two more reflections suffice for some light to get through the SMEI aperture at Z0. This light is a diffuse glow on the rear of Z3 and is important, as discussed just before §IV-A, when subsequent optics-box background rejection is included, only when within about a centimeter of the Z3 vane edge.

With the 52 mm lens focussed on the rear of Z3, one CCD pixel is ~0.05 mm. The ~1 cm wide band around Z3 mentioned above in §IV occupies ~10^6 pixels, ten times the area the CCD is actually able to observe. The reading within the CCD's FOV must be corrected by this appropriate factor to yield the correct r_1 in eq(3).

To increase the amount of scattered laser light, a hole punch was used to make a 0.6 cm diameter white-paper disk. This was attached to a length of black thread, which was manipulated through the baffle-front opening to deposit the disk at various locations within the S6 → S8

septum bottoms. When illuminated with the laser spot, this disk provided a 40-fold increase in scattered laser light, which enabled the detection of the diffuse glow on the rear of Z3, but only when the opening in Z3 could directly view the disk. This glow was uniform from side to side of the rear of Z3, and varied no more than a factor of two from top to bottom.

Septum bottoms at the narrow ends of the baffle are the only ones directly viewed through the Z3 opening. For these, a typical rear-Z3 diffuse-glow measurement was 0.015 ADUs/pixel, after correction for the presence of the white spot. Multiplying by the above 10^6 pixels yields r = 15,000: the fraction of light leaving the rear of vane Z3 and passing through Z0 is $\sim 10^{-11}$ for septum positions with a good view of the opening in Z3. Background-light levels diminish when the spot is hidden from the Z3 opening by another vane; this defines the effective area A_i for each of the three septum regions. Total area ($\Theta_y = 0$) grows from zero at $\Theta_x = 90°$ to a maximum of ~ 100 cm^2 at $\Theta_x = 65°$. Resulting $\sum R_i$ depends on $[\Theta_x, \Theta_y]$, but at most is 6×10^{-10}.

VIII. DIRECT ILLUMINATION THROUGH THE Z3 OPENING

The diffuse glow on the rear of Z3 is an easy-to-see ~ 15 ADUs per pixel when the laser beam illuminates the front of vanes Z2, 1, or 0 through the opening in Z3. This indicates about 10^{-8} of the laser light leaves the 1 cm wide band of Z3 to pass through Z0, roughly as expected given two Martin-Black reflections each at 1% reflectivity and the solid-angle restrictions on the two scatterings. When the laser illuminates the Z3 edge directly, about 10^{-6} of the light passes through the Z0 aperture. Typical R_t here are respectively $\sim 2 \times 10^{-7}$ and 5×10^{-7}.

IX. UPPER LIMIT ON SCATTERING FROM THE Z0 EDGE

Light can scatter from the edge of Z0 directly into the SMEI FOV. Given the Z0 edge area is several percent of its aperture area, reflectivity 1%, and solid angle for scattering into a given square degree of the SMEI FOV on the CCD is $\sim 5 \times 10^{-5}$ of the total, we expect an efficiency of $\sim 10^{-8}$ for this mechanism, two decades below the R_{optics} upper limit at large θ (§IV). Although likely negligible for SMEI, it is prudent to check with the prototype baffle. For this, the CCD camera was moved back to focus on Z0 rather than Z3. It was then centered on the baffle center line and its aperture reduced just enough to exclude direct view of either Z3 vane edges. The laser beam was positioned as in §V to produce the maximum Z6-to-Z3 bright edge. No Z0 edge was seen, ≤ 50 ADUs for all pixels combined along the edge, a reduction of 10^{-4} on the R_{Z6} of §V, and $R_{tot} \leq 2 \times 10^{-16}$ when the requisite division by Ω_{FOV} is included. Similarly, a limit of ≤ 20 ADUs is set with the laser beam as in §VIII illuminating through the Z3 opening. In this case, $\leq 10^{-11}$ of the laser beam is seen on the Z0 edge, again reduced by 10^{-4} or more as above. These limits are a factor of ten above the amounts of light expected, but they suffice to prove that this mechanism's impact on SMEI is negligible.

X. COMBINING MEASUREMENTS INTO A MODEL OF BAFFLE PERFORMANCE

Figure 2 shows baffle-performance domains versus $[\Theta_x, \Theta_y]$. Performance changes dramatically as incident light moves from one domain to another, since the dominant stray-light

41

Light-rejection performance domains of the SMEI baffle
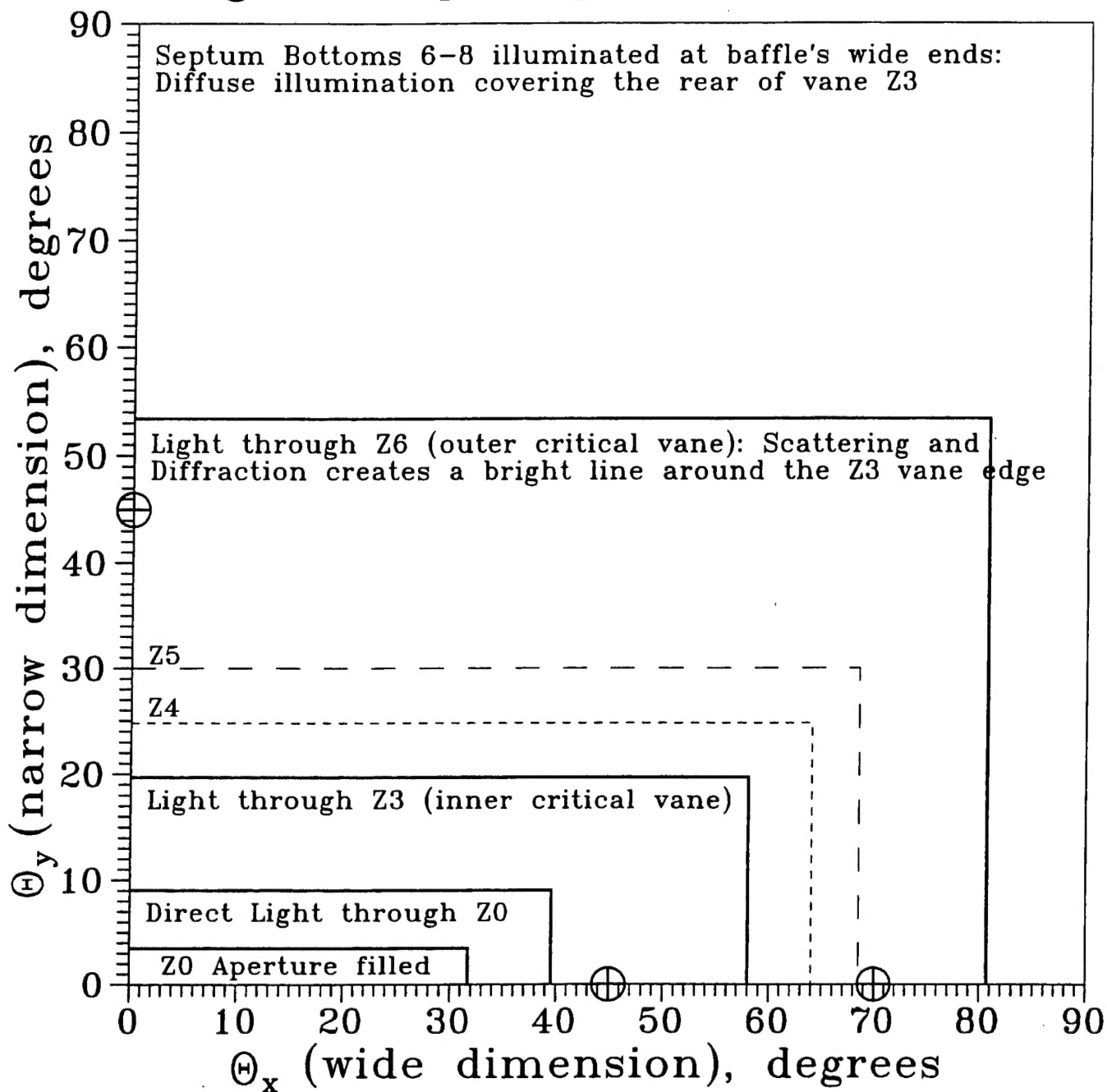
$\oplus$: White-light, large-area confirmations

Septum Bottoms 6-8 illuminated at baffle's wide ends:
Diffuse illumination covering the rear of vane Z3

Light through Z6 (outer critical vane): Scattering and
Diffraction creates a bright line around the Z3 vane edge

Z5

Z4

Light through Z3 (inner critical vane)

Direct Light through Z0

Z0 Aperture filled

Θ_y (narrow dimension), degrees

Θ_x (wide dimension), degrees

Figure 2. Light-rejection performance domains of the SMEI baffle as a function of the incident light angles Θ_x (wide dimension) and Θ_y (narrow dimension). The origin of coordinates is the baffle center line. Background-light level within each rectangular box is dominated by the mechanism indicated near the boundary. The three $\oplus$ symbols indicate the locations at which the results from equation (3) presented in the next two figures were checked using the white-light source and equation (1).

SMEI BAFFLE PERFORMANCE
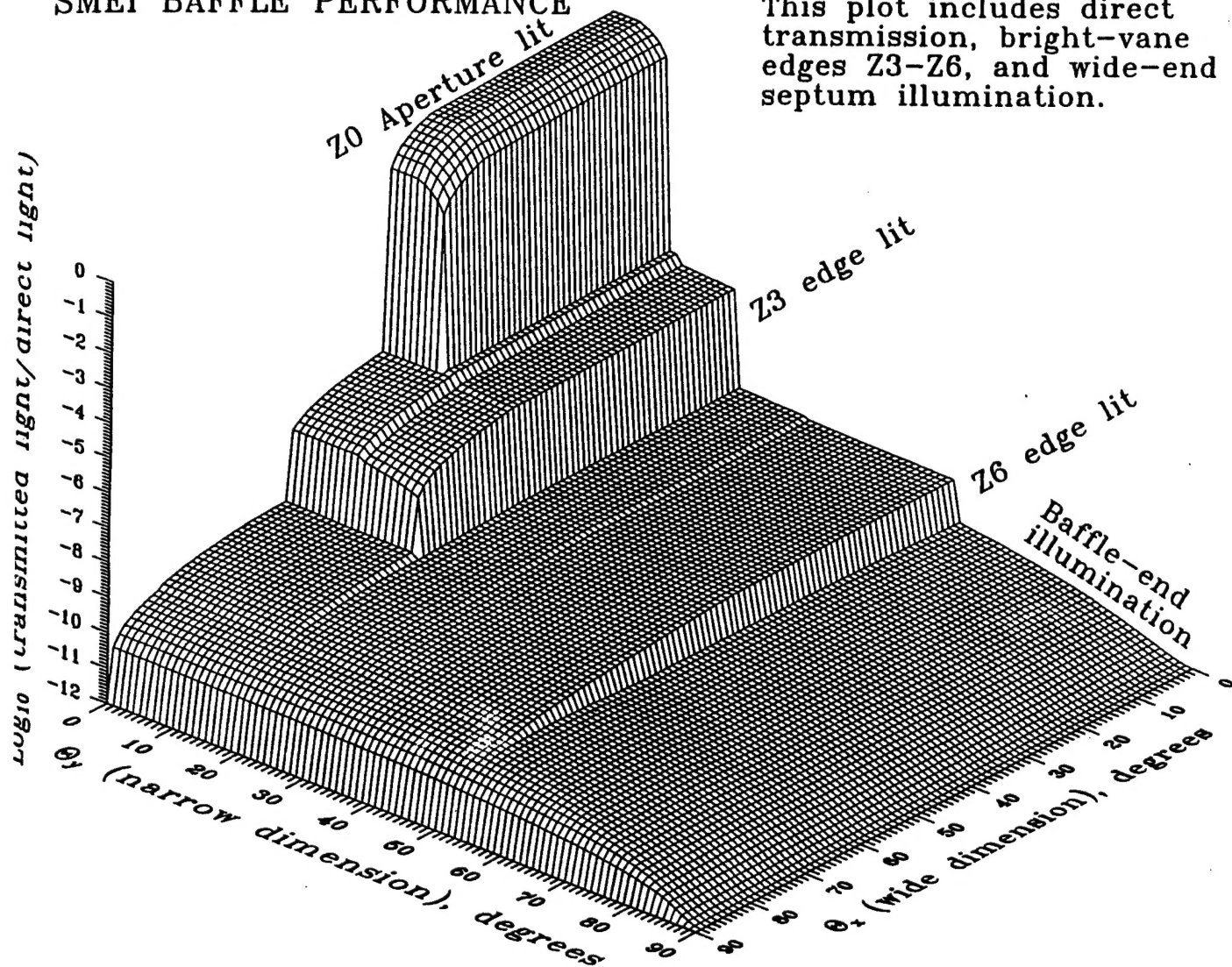
This plot includes direct transmission, bright-vane edges Z3-Z6, and wide-end septum illumination.

Figure 3. Plot of SMEI baffle performance as a function of incident-light angles. Evaluated by equation (3), using discrete laser-light measurements and calculated illuminated areas.
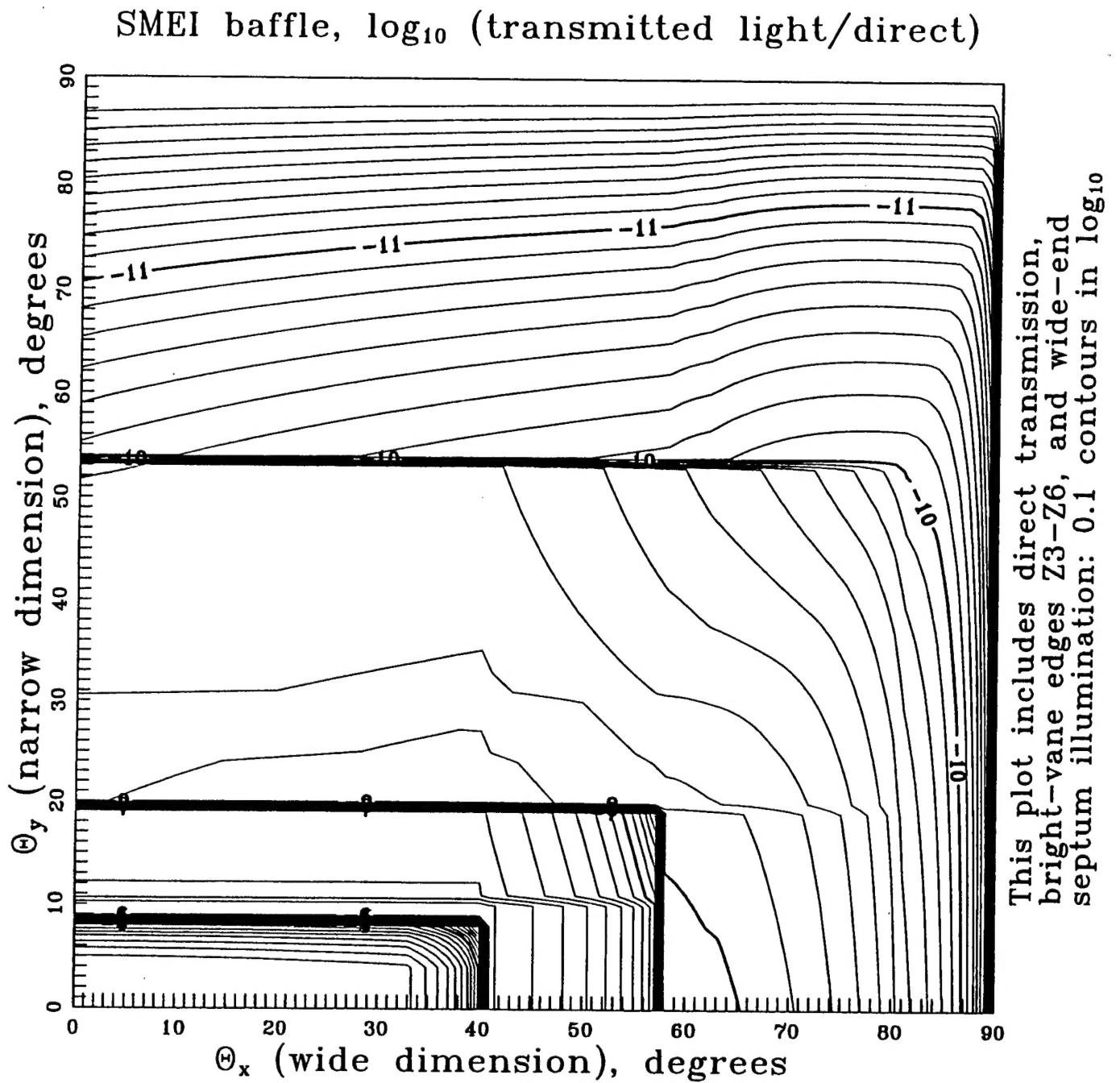
SMEI baffle, $\log_{10}$ (transmitted light/direct)

This plot includes direct transmission, bright–vane edges Z3–Z6, and wide–end septum illumination: 0.1 contours in $\log_{10}$

Θ_y (narrow dimension), degrees

Θ_x (wide dimension), degrees

Figure 4. Same as figure 3, but a contour plot. Contour intervals here: 0.1 in $\log_{10}$ of R_b (Θ_x, Θ_y) as calculated from equation (3).

mechanism depends critically on which vane edges and interior septums are illuminated. For each of these domains the appropriate $A_i(\Theta_x, \Theta_y)$ is calculated, including 3-dimensional shadowing of outer vanes on the illumination of interior vane edges and septum bottoms, and paired with the appropriate r_i, to evaluate eq(3). Figures 3 and 4 present the results. Figure 2 also shows three (Θ_x, Θ_y) locations at which these results were confirmed by white-light measurements with eq(1).

XI. SUMMARY AND DISCUSSION

The SMEI prototype baffle provides background-light rejection between one and two decades improved over the $\sim 10^{-8}$ delivered by its predecessor, the earlier prototype baffle. Addition of secondary vanes, especially Z4 and Z5 blocking Z3's view of nearby septum bottoms, enabled the improvement. Moreover, adding vanes Z1 and Z2 (blocking both illumination and viewing of septum bottoms between Z0 and Z3) significantly reduces light coming through Z0 at wide angles, $\theta \gtrsim 40°$, which was plentiful in the earlier baffle. Although the $\sim 10^{-9}$ overall performance close to the design angles $(\Theta_x, \Theta_y) = (20°, 60°)$ realized here is about a decade higher than the original SMEI specification, better than specification performance in the SMEI optics-box light rejection should just about make up the difference. However, we note if the baffle degrades significantly due to contamination or other changes over time, the $R_{tot} < 10^{-15}$ end-to-end specification will probably also be breached.

As the interior of the baffle is more deeply illuminated, increasing amounts of stray light pass through the main SMEI aperture, the opening in vane Z0. Figures 3 and 4 provide a quantitative means of evaluating the background-light impact on SMEI, of protruding illuminated spacecraft appendages and of the Earth horizon, Moon and Sun. Moreover, when the Sun illuminates within Z3, we now know at least $\sim 3 \times 10^{-7}$ of sunlight will pass through Z0, having reflected from the front of vane Z0 and again from the 1 cm wide band around the opening, on the rear of Z3. Considerably more light in this case could pass through Z0 at wider angles, $\theta \gtrsim 40°$. We expect all this light will be further reduced within the optics box, to a typical background surface brightness on the CCD of about 300 S10. This is about 1% the brightness of zodiacal light at elongation $\epsilon = 10°$, which is the closest SMEI can look to the Sun without allowing some direct sunlight through Z0. At $\epsilon = 20°$ the zodiacal light is fivefold less than at 10°. Thus, for heliospheric features which are 1% the brightness of the zodiacal light for $10° < \epsilon < 20°$, the SMEI background-light ranges from comparable to five times larger.